

Luttinger's Theorem Violation and Green's Function Topological Invariants in a Fractional Chern Insulator

Anton A. Markov^{¶,1,2,3,*} Andrey M. Nikishin^{¶,3,4,†} Nigel R. Cooper,⁵ Nathan Goldman,^{1,2,6,‡} and Lucila Peralta Gavensky^{1,2,§}

¹International Solvay Institutes, 1050 Brussels, Belgium

²Center for Nonlinear Phenomena and Complex Systems, Université Libre de Bruxelles (U.L.B.), B-1050 Brussels, Belgium

³Russian Quantum Center, Moscow 121205, Russia[¶]

⁴Moscow Institute of Physics and Technology, Institutsky lane 9, Dolgoprudny, Moscow region, 141700

⁵T.C.M. Group, Cavendish Laboratory, University of Cambridge, J.J. Thomson Avenue, Cambridge CB3 0US, United Kingdom

⁶Laboratoire Kastler Brossel, Collège de France, CNRS, ENS-Université PSL, Sorbonne Université, 11 Place Marcelin Berthelot, 75005 Paris, France

(Dated: March 19, 2026)

Luttinger's theorem constrains the particle density of interacting fermions through global properties of the single-particle Green's function, and its violation signals a breakdown of the identification between the quantized Hall response and the Green-function-based Ishikawa-Matsuyama invariant. This phenomenon becomes especially compelling in strongly correlated topological phases, such as fractional Chern insulators, where fractionalized quasiparticles lack an adiabatic connection to electrons, raising the question of how Green's-function-based topological invariants manifest in such phases. Using exact diagonalization of the fermionic Harper-Hofstadter-Hubbard model, we compute bulk single-particle Green's functions deep inside a fractional Chern insulating phase and directly evaluate the Luttinger count, its possible correction (the Luttinger integral), and the Ishikawa-Matsuyama invariant $N_3[G]$. We demonstrate a clear violation of Luttinger's theorem and show that the fractional nature of the many-body Chern number is encoded in the Středa response of the Luttinger integral, while the integer invariant $N_3[G]$ arises from the Středa response of the Luttinger count. We also analytically prove that $N_3[G]$ is fully determined by the Luttinger count together with the Chern number of the occupied Bloch band, upon neglecting Bloch-band mixing. Finally, we propose an experimental protocol to extract all Green-function-based topological invariants from local density-of-states measurements, experimentally accessible in fractional quantum Hall systems.

I. INTRODUCTION

The success of many-body perturbation theory relies on the assumption of adiabatic continuity between electrons and low-energy quasiparticle excitations [1, 2]. In such cases, the single-particle Green's function, which describes electron propagation through a many-body system, encodes detailed information about these low-energy degrees of freedom. The situation is markedly different in Fractional Quantum Hall (FQH) [3] states and their lattice counterparts, Fractional Chern Insulators (FCIs) [4]. In these systems, the fundamental low-energy quasiparticles carry fractional charge and lack an adiabatic connection to the physical electrons [5]. Nevertheless, theory predicts that bulk single-electron excitations of the FQH liquid remain well defined and long lived, though they occur only at high energies [6–8]. These theoretical predictions have recently gained renewed attention [9–12], motivated in part by new scanning tunneling microscopy measurements of FCI spectral densities in graphene [13] and moiré materials [14]. This progress raises a central question: if the single-particle Green's

function primarily probes the high-energy sector of FQH physics, how much information can it reveal about the system's low-energy topological order?

Topological properties of non-interacting (and weakly-interacting) quantum matter are known to be encoded in the topology of their single-particle Green's functions [15–17]. In particular, Ishikawa and Matsuyama [15] proposed that the quantized Hall conductivity of two-dimensional insulators can be expressed as $\sigma_H = (e^2/h)N_3[G]$, where $N_3[G]$ denotes a topological invariant built from the single-particle Green's function $G(\mathbf{k})$:

$$N_3[G] = \frac{\epsilon^{\mu\nu\gamma}}{24\pi^2} \int d^3k e^{k_0 0^+} \text{Tr} \left(G^{-1} \frac{\partial G}{\partial k_\mu} G^{-1} \frac{\partial G}{\partial k_\nu} G^{-1} \frac{\partial G}{\partial k_\gamma} \right). \quad (1)$$

Here $G(\mathbf{k})$ denotes the Matsubara Green's function, $\mathbf{k} = (i\omega, k_x, k_y)$ is a three-vector in frequency-momentum space, $\epsilon^{\mu\nu\gamma}$ is the Levi-Civita symbol and the trace runs over all internal degrees of freedom. The initial derivation of Ref. [15] appeared to be non-perturbative, relying only on Ward-Takahashi identities [18, 19], which led to the expectation that the relation $\sigma_H = (e^2/h)N_3[G]$ should persist beyond the weakly-interacting regime. However, the integer nature of $N_3[G] \in \mathbb{Z}$ suggests that the Ishikawa-Matsuyama relation should break down in the FQH regime, where the Hall conductivity is known to be fractionally quantized according to the many-body Chern number $\sigma_H = (e^2/h)C^{\text{MB}}$ [20, 21]. The possible multivaluedness of the

* anton.markov@ulb.be

† a.nikishin@rqc.ru

‡ nathan.goldman@lkb.ens.fr

§ lucila.peralta.gavensky@ulb.be

¶ These authors contributed equally to this work.

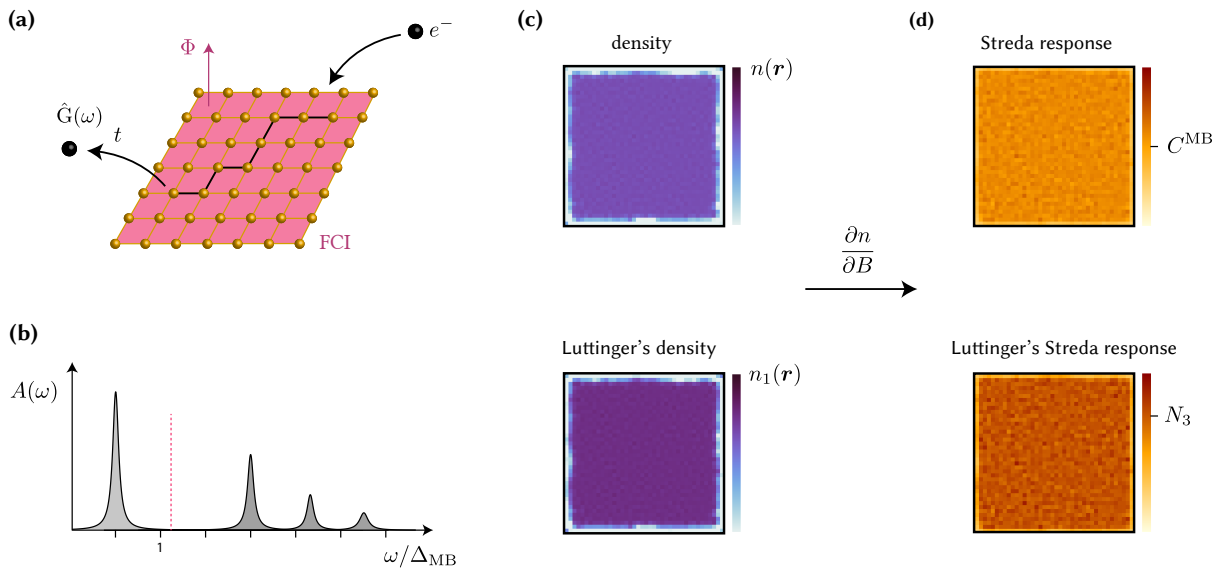


FIG. 1. **Schematic illustration of the system, approach and key results.** (a) We study the bulk single-particle Green's function $G(\omega)$ of interacting electrons in a uniform magnetic field realizing a fractional Chern insulator. (b) Schematic spectral function of a FQH state. The electronic spectral density exhibits sharp coherent hole-like and electron-like peaks, corresponding to long-lived charged excitations located well above the neutral many-body gap Δ_{MB} . The dashed red line indicates the emergence of a zero of G within the charge gap. (c) In the FCI phase, the particle density and the Luttinger-count density differ, signaling a violation of Luttinger's theorem. (d) The Středa response of the particle density evaluated deep within the bulk yields the fractional many-body Chern number C^{MB} , whereas the Středa response of the Luttinger-count density n_1 produces an integer valued $N_3[G]$ different from C^{MB} .

Green's functions [15, 22] was proposed as a way to reconcile the apparent discrepancy between the integer quantization of $N_3[G]$ and the fractionally quantized values of the Chern number C^{MB} in the strongly-correlated FQH regime. In later years, the equivalence between $N_3[G]$ and the many-body Chern number was cast into doubt. While C^{MB} cannot change without the collapse of the many-body gap, $N_3[G]$ can change when a zero of the single-particle Green's function crosses the chemical potential [23]. In fact, deviations between $N_3[G]$ and C^{MB} were explicitly demonstrated, in both numerical and analytical studies [24–29]. For FQH states, the discrepancy was shown indirectly in Ref. [24], by invoking the bulk-edge correspondence [30], and relying on the Green's functions of an effective low-energy edge theory [31]. More recently, Ref. [28] clarified that the original Ishikawa-Matsuyama relation [15] implicitly relied on perturbative assumptions.

These developments raise fundamental questions about the physical significance of the $N_3[G]$ invariant in strongly-interacting topological matter, both in systems lacking genuine topological order [25, 26] and in topologically-ordered (FQH and FCI) phases [24, 32]. A recent advance in this direction was made in Ref. [27], which reformulated $N_3[G]$ within the framework of Luttinger's theorem [2] and the Středa-Widom relation [33, 34]. In Luttinger and Ward's original proof, [2] the total particle number N is split into the Luttinger count $N_1[G]$ and the Luttinger integral ΔN_1 . In a Fermi liquid, $N_1[G]$ counts the number of single-particle states available to quasiparticles, whereas the Luttinger integral vanishes. Ref. [27] applied an analogous decomposition to the Středa-Widom relation

[33, 34], which states that $C^{MB} = \Phi_0 \partial N / \partial \Phi$, with $\Phi_0 = hc/e$ the flux quantum and Φ the total flux threading the system. Within this viewpoint, N_3 captures the Středa response of the Luttinger count $\Phi_0 \partial N_1 / \partial \Phi$ [98]. Thus, the many-body Chern number is equal to N_3 provided the Luttinger integral vanishes and Luttinger's theorem holds. The possible breakdown of Luttinger's theorem in strongly-correlated quantum matter has been intensely studied over the past decades [28, 36–46], and the precise conditions for this violation have been a subject of intense debate [45, 46]. In particular, pioneering works already revealed non-zero values of the Luttinger integral ΔN_1 in different settings, including antiferromagnetic metals [38] and in the Sachdev–Ye–Kitaev model [39]. For the purpose of our work, a key insight from this literature is that Luttinger's theorem can fail when the single-particle Green's function develops zeros [28, 36–38, 40, 42–44, 47–50].

Despite this progress, a direct evaluation of Green's-function-based topological invariants deep within the bulk of a fractionalized phase has remained elusive. This manuscript closes that gap by presenting a direct calculation of single-particle Green's functions in the bulk of an FCI state realized in the fermionic Harper-Hofstadter-Hubbard model [51, 52], obtained via exact diagonalization. We demonstrate the breakdown of Luttinger's theorem in this setting by explicitly evaluating N_1 and ΔN_1 , providing what is, to the best of our knowledge, the first exact numerical computation of these quantities in a strongly correlated topological phase. We then show – both analytically and numerically – that the fractional character of the many-body Chern number C^{MB}

is encoded in the Středa response of the Luttinger integral, $\Phi_0 \partial(\Delta N_1)/\partial\Phi \in \mathbb{Q}$, rather than in the Středa response of the Luttinger count, $\Phi_0 \partial N_1/\partial\Phi = N_3 \in \mathbb{Z}$. Thereafter, we show analytically that N_3 is fully determined by the Luttinger count N_1 together with the single-particle Chern numbers of the occupied Bloch bands, provided interaction-induced Bloch-band mixing is neglected. Finally, we propose a protocol for extracting the Luttinger count, the Luttinger integral and their Středa response from the probes of the local density of states, now available experimentally for FCI states [13, 14]. A schematic summary of our approach and main results is shown in Fig. 1.

The manuscript is organized as follows. In Section II, we review the relation between topological invariants of the single-particle Green's function and Luttinger's theorem. In Section III, we characterize the bulk single-particle spectral properties of the FCI, identifying the emergence of poles and zeros of the Green's function; we then present numerical evidence for the violation of Luttinger's theorem, and obtain the individual Středa responses of the bulk particle density and its Luttinger constituents (i.e. the local Luttinger's count and integral). In Section IV we provide an analytical framework that rationalizes these numerical findings, deriving an explicit expression for N_3 in the absence of Bloch band mixing. In Section V, we propose a practical scheme for extracting the Luttinger's count and integral, and their Středa responses, from local density of states measurements. We conclude in Section VI with a discussion of the implications of our findings and possible future research directions.

II. PARTICLE COUNTING, LUTTINGER'S THEOREM AND TOPOLOGICAL WINDING NUMBERS OF THE GREEN'S FUNCTION

The particle number of an interacting system at a given chemical potential μ and zero temperature can be expressed in terms of the single-particle Green's function as

$$N(\mu) = \frac{1}{2\pi i} \int dz e^{z0^+} \text{Tr}[G(z)] = \int_{-\infty}^{\mu} d\omega A(\omega), \quad (2)$$

where $G(z)$ is defined on the complex frequency plane and the integral in the first equality is understood as a principal value taken along a line parallel to the imaginary axis, $z = \mu + i\omega'$. The second equality is obtained by deforming the contour toward the real axis, $z = \omega \mp i0^+$, which naturally defines the total spectral density or density of states

$$A(\omega) = \sum_{\alpha} A_{\alpha}(\omega) = \frac{1}{\pi} \sum_{\alpha} \text{Im} G_{\alpha\alpha}(\omega - i0^+), \quad (3)$$

with $A_{\alpha}(\omega)$ the contribution from state α .

Following Luttinger and Ward [2], Eq. (2) can be decomposed into two terms: the Luttinger count $N_1[G]$, which depends solely on the analytical structure of the propagator, and the Luttinger integral ΔN_1 , which explicitly

involves the self-energy $\Sigma(z)$,

$$N = N_1[G] + \Delta N_1, \quad (4a)$$

$$N_1[G] = -\frac{1}{2\pi i} \int dz e^{z0^+} \text{Tr}[G^{-1}(z) \partial_z G(z)], \quad (4b)$$

$$\Delta N_1 = \frac{1}{2\pi i} \int dz e^{z0^+} \text{Tr}[G(z) \partial_z \Sigma(z)]. \quad (4c)$$

Luttinger's theorem holds whenever $\Delta N_1 = 0$, in which case the particle number is entirely determined by $N_1[G]$ [2]. Crucially, when $G(z)$ has no poles or zeros at the chemical potential, the contour in Eq. (4b) can be closed in the lower half-plane, turning the Luttinger count into a bona-fide topological invariant: the first-order winding number of the Green's function [23, 53]. To clarify what this topological count actually evaluates in an interacting system, it is useful to make explicit the analytical structure of $G(z)$. For a finite system, each diagonal element has the rational form [53],

$$G_{\alpha\alpha}(z) = \sum_p \frac{Z_{\alpha}^{(p)}}{z - \varepsilon_{\alpha}^{(p)}} = \frac{\prod_s (z - \chi_{\alpha}^{(s)})}{\prod_p (z - \varepsilon_{\alpha}^{(p)})}, \quad (5)$$

where $Z_{\alpha}^{(p)} > 0$ are the Lehmann spectral weights, and $\varepsilon_{\alpha}^{(p)}$ and $\chi_{\alpha}^{(s)}$ denote the poles and zeros of $G_{\alpha\alpha}(z)$, respectively. In this structure, each zero necessarily lies between two consecutive poles along the real-frequency axis, reflecting the redistribution of spectral weight induced by interactions. Figure 2(a) illustrates this behavior schematically. Choosing α to label the basis that diagonalizes $G(z)$, the Luttinger count becomes

$$N_1[G] = \sum_{\alpha} \int_{-\infty}^{\mu} d\omega n_{1\alpha}(\omega), \quad (6)$$

with the Luttinger counting kernel

$$n_{1\alpha}(\omega) = \sum_p \delta(\omega - \varepsilon_{\alpha}^{(p)}) - \sum_s \delta(\omega - \chi_{\alpha}^{(s)}), \quad (7)$$

so that each pole below μ contributes +1, while each zero contributes -1. Because these contributions are discrete, the only way to modify this quantized invariant is for a pole or a zero to cross the chemical potential. Figure 2(b) compares $A_{\alpha}(\omega)$ and $n_{1\alpha}(\omega)$ for the toy Green's function of Fig. 2(a). Taking, for instance, $\mu = 0$, one immediately sees how Luttinger's theorem can fail in a correlated insulator even in the absence of Green's functions zeros below the chemical potential: the spectral density $A_{\alpha}(\omega)$ integrates to the actual spectral weight of the peak below μ , while the Luttinger count assigns that peak a unit weight. It is also important to note that, if the chemical potential is allowed to vary within the single-particle gap, the Luttinger count value changes by ± 1 when a Green's function zero crosses the Fermi level [40].

In the absence of poles and zeros at the chemical potential, Ref. [27] further showed that the Ishikawa-Matsuyama invariant $N_3[G]$ can be accessed directly by evaluating the Středa response of the Luttinger count $N_1[G]$:

$$N_3[G] = \Phi_0 \left. \frac{\partial N_1[G]}{\partial\Phi} \right|_{\mu}, \quad (8)$$

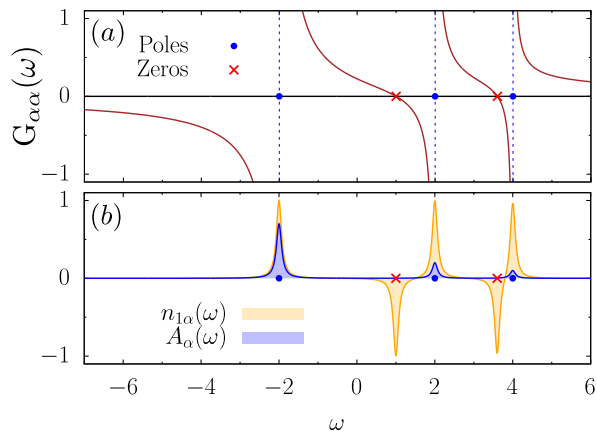


FIG. 2. (a) Schematic illustration of the diagonal element of a toy single-particle Green's function on the real-frequency axis, with poles at $\varepsilon_\alpha^{(p)} = -2, 2, 4$ (blue circles) and corresponding spectral weights $Z_\alpha^{(p)} = 0.7, 0.2, 0.1$. The positions of the zeros $\chi_\alpha^{(s)}$ of $G_{\alpha\alpha}(\omega)$ are indicated by red crosses. (b) Spectral density $A_\alpha(\omega)$ [Eq. (3)] and Luttinger counting kernel $n_{1\alpha}(\omega)$ [Eq. (7)].

i.e., by monitoring how the Luttinger count responds to an infinitesimal flux Φ threading the system at fixed chemical potential μ . This relation circumvents the need to evaluate the full three-form defining $N_3[G]$, allowing one to work entirely at the level of the one-form Luttinger sum rule. When Luttinger's theorem is violated ($\Delta N_1 \neq 0$), the discrepancy between the many-body Chern number and the Green's function based-invariant is then captured by the flux derivative of the Luttinger integral,

$$\Delta N_3 = C^{\text{MB}} - N_3[G] = \Phi_0 \left. \frac{\partial \Delta N_1}{\partial \Phi} \right|_\mu. \quad (9)$$

In what follows, we exploit this connection by numerically evaluating $N_1[G]$, ΔN_1 , and their flux derivatives in a fractional Chern insulator, enabling a direct diagnosis of both the breakdown of Luttinger's theorem and an exact evaluation of these Green's function-based topological invariants in a topologically ordered system from exact diagonalization calculations.

III. GREEN'S FUNCTION AND TOPOLOGICAL INVARIANTS FROM EXACT DIAGONALIZATION

In view of performing explicit numerical calculations, we henceforth consider the Harper-Hofstadter-Hubbard model, paradigmatic model for FCI states [51, 52]. The model describes a system of N interacting spinless fermions subjected to a uniform magnetic field with the Hamiltonian:

$$H = \sum_{n,m} \left[-t \left(c_{n,m+1}^\dagger c_{n,m} + c_{n+1,m}^\dagger c_{n,m} e^{i2\pi m\varphi} + h.c. \right) + V \hat{P} : n_{n,m} (n_{n\pm 1,m} + n_{n,m\pm 1}) : \hat{P} \right], \quad (10)$$

where $c_{n,m+1}^{(\dagger)}$ annihilates (creates) a fermion on the lattice site (n, m) , φ is the magnetic flux per plaquette in units of the flux quantum, V is the nearest neighbor interaction strength, $:$ stands for the normal ordering and \hat{P} projects the dynamics onto the lowest Hofstadter band (LHB). In the weak magnetic field regime $\varphi \ll 1$, the LHB continuously connects to the lowest Landau Level. At fractional fillings $\nu = N/N_\Phi$, where N_Φ is the number of flux quanta piercing the system, the projected interacting model supports fractional Chern insulator phases, that closely resemble the corresponding Laughlin states in the continuum [4, 54].

To investigate the fate of the Luttinger's theorem and the Ishikawa-Matsuyama invariant in these fractional Chern insulator states, we proceed in two complementary ways. First, we study the system in a finite box with open boundary conditions and compute the single-particle Green's function $G(\mathbf{r}, \mathbf{r}'; z)$ and self-energy $\Sigma(\mathbf{r}, \mathbf{r}'; z)$ using Lanczos exact diagonalization (see Section A for details). This approach allows us to evaluate spatially resolved versions of the Luttinger count and integral in Eq. (4),

$$n_1(\mathbf{r}) = -\frac{1}{2\pi i} \int_{\mathcal{C}} dz \sum_{\mathbf{r}'} G^{-1}(\mathbf{r}, \mathbf{r}'; z) \partial_z G(\mathbf{r}', \mathbf{r}; z) \quad (11)$$

$$\Delta n_1(\mathbf{r}) = \frac{1}{2\pi i} \int_{\mathcal{C}} dz \sum_{\mathbf{r}'} \partial_z \Sigma(\mathbf{r}, \mathbf{r}'; z) G(\mathbf{r}', \mathbf{r}; z),$$

where the contour \mathcal{C} encloses all occupied poles in the complex frequency plane. In the bulk region, the insulating gap ensures that both G and Σ decay exponentially with $|\mathbf{r} - \mathbf{r}'|$, according to a finite correlation length, see Appendix B. Evaluating these quantities deep within the bulk region therefore provides a faithful representation of the intrinsic bulk response to a magnetic perturbation, see Eqs. (8) and (9).

As a second, complementary approach, we apply the same exact diagonalization method to the Hamiltonian defined on a torus. While the Středa response is hard to probe in this geometry due to the Dirac quantization of the magnetic flux, the torus preserves translational invariance and eliminates edge effects, allowing us to benchmark the results extracted from the bulk of the open-boundary box. It also enables investigation of the momentum dependence of $G(\mathbf{k}; z)$ and $\Sigma(\mathbf{k}; z)$, a key aspect for elucidating the behavior of the winding number $N_3[G]$.

We focus on the most stable fractional Chern insulating phase for fermions, which occurs at filling $\nu = \frac{1}{3}$. To realize this state, we consider a magnetic flux per plaquette $\varphi = \frac{1}{5}$, corresponding to a nearly flat LHB that closely resembles the lowest Landau level. For the simulations, we consider $N_p = 6$ particles on a finite open-boundary box of $N_x \times N_y = 11 \times 10$ sites, while the torus geometry has $N_x \times N_y = 9 \times 10$ sites, covering the same total area. The interaction strength is set to $V/t = 10$. This choice of parameters stabilizes the same phase in both geometries as we demonstrate below.

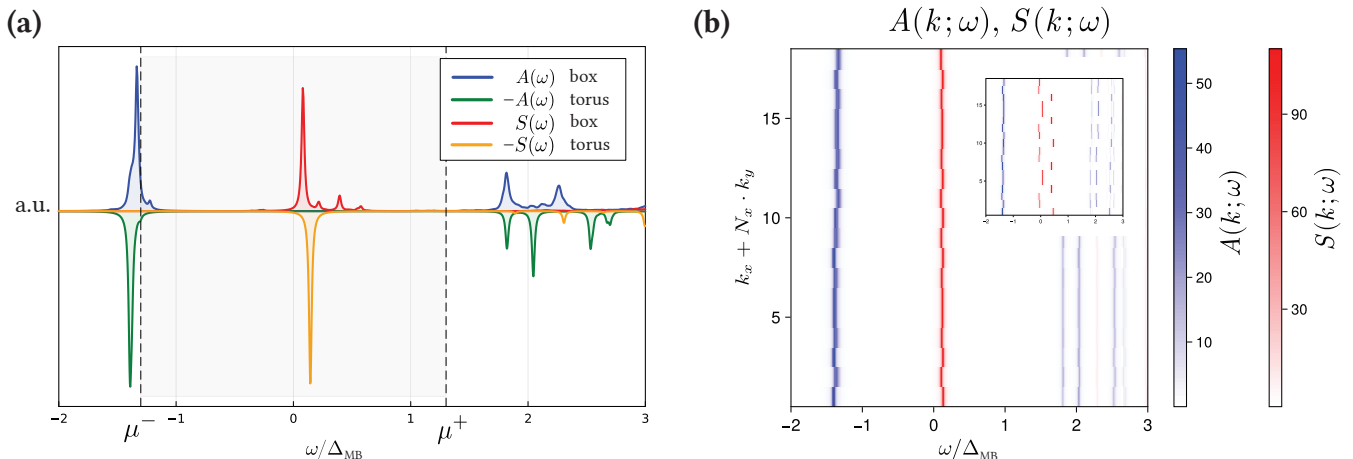


FIG. 3. **Analytical structure of the Green's functions and the self-energy.** (a) Local spectral densities of the Green's function, $A(\omega)$, and the self-energy, $S(\omega)$, defined in Eq. (12) computed in the finite box (positive sign) and on the torus (negative sign). Dashed lines denote the electron addition and removal energies, $\mu^+ = E_0(N+1) - E_0(N)$ and $\mu^- = E_0(N) - E_0(N-1)$, extracted from the torus geometry, where $E_0^{N\pm 1}$ are the ground state energies in the $N \pm 1$ -particle sectors. Note that $A(\omega)$ and $S(\omega)$ are plotted in different scales. (b) Momentum-resolved spectral densities $A(k; \omega)$ and $S(k; \omega)$ on the torus geometry. The main panel shows spectra obtained from the thermodynamically averaged Green's function over the degenerate ground-state manifold [Eq. (13)], while the inset presents the result of averaging only over a single ground-state [Eq. (14)]. The frequency is measured in units of the fixed- N many-body gap Δ_{MB} computed on the torus geometry, with zero frequency set at $(\mu^+ + \mu^-)/2$. The momenta k_x and k_y are measured in units of $\frac{2\pi}{N_x}$ and $\frac{2\pi}{qN_y}$.

A. Bulk Green's Functions of a Laughlin-type FCI state

We begin by characterizing the bulk properties of the system through the frequency dependence of the retarded Green's function and the self-energy. To this end, we focus on the corresponding local spectral densities,

$$\begin{aligned} A(\omega) &= -\frac{1}{\pi} \text{Im} [G(\mathbf{r}_0, \mathbf{r}_0; \omega + i0^+)] \\ S(\omega) &= -\frac{1}{\pi} \text{Im} [\Sigma(\mathbf{r}_0, \mathbf{r}_0; \omega + i0^+)], \end{aligned} \quad (12)$$

with the site \mathbf{r}_0 chosen at the center of the sample. In the bulk, the residual dependence of $A(\omega)$ and $S(\omega)$ on the spatial coordinate \mathbf{r}_0 arises solely due to finite-size effects, and can therefore be neglected [99]. However, in a small finite-size box, the self-energy spectral density becomes particularly sensitive to edge effects, even though the correlation length for our parameter set is only on the order of a single lattice constant; see Section B. In this sense, a comparison with the results obtained on the torus geometry are relevant.

The spectral densities $A(\omega)$ and $S(\omega)$ provide complementary information: $A(\omega)$ resolves the poles of the Green's function and thus the single-particle density of states, whereas $S(\omega)$ captures the location of its zeros. The resulting spectra are shown in Fig. 3. Panel (a) displays $A(\omega)$ and $S(\omega)$ for both box and torus geometries as a function of frequency ω , with the torus data plotted with opposite sign for ease of comparison. Interactions split the quasi-flat single-particle LHB, opening a clear charge gap that separates the density of states corresponding to electron removal (occupied states) from that corresponding to electron

addition (empty states). Crucially, this gap is accompanied with the emergence of a single zero of the Green's function (or equivalently, a pole in the self-energy), visible as a peak in $S(\omega)$. This pole-zero structure reflects a strong redistribution of spectral weight induced by the correlations.

Remarkably, the spectral function $A(\omega)$ exhibits sharp, coherent features: a dominant hole-like peak and several pronounced electron-like peaks, superimposed on a weaker incoherent background, indicating the presence of well-defined, long-lived high-energy quasiparticle excitations. The overall structure, and its pronounced particle-hole asymmetry, closely mirror previous results obtained for FQH states on the sphere [8, 9, 56–58]. In particular, the strong asymmetry between the hole and particle sectors, first noticed in Ref. [56], is a hallmark of Laughlin-type fractionalized states and reflects the fundamentally different nature of quasiholes and quasielectrons [59]. Physically, the simplicity of the hole sector for this particular filling reflects the fact that for a $\frac{1}{m}$ -Laughlin state removing an electron is exactly equivalent to inserting m quasi-hole excitations [59]. The resulting state is therefore very close to an eigenstate of the many-body Hamiltonian, which leads to a single coherent peak on the hole side [56]. In contrast, an inserted electron decomposes into multiple excitations that cannot be represented by a unique low-energy eigenstate. This fragmented particle-side spectrum, with a small number of dominant coherent peaks, has been understood within the composite-fermion framework [8, 9, 58]. Notably, in our bulk box calculations we observe two pronounced particle-like peaks, in close correspondence with the results for $\nu = 1/3$ in Refs. [8, 9, 58]. On the torus, the particle side of the spectrum is more involved as first noted in Ref. [12]. However, the difference between

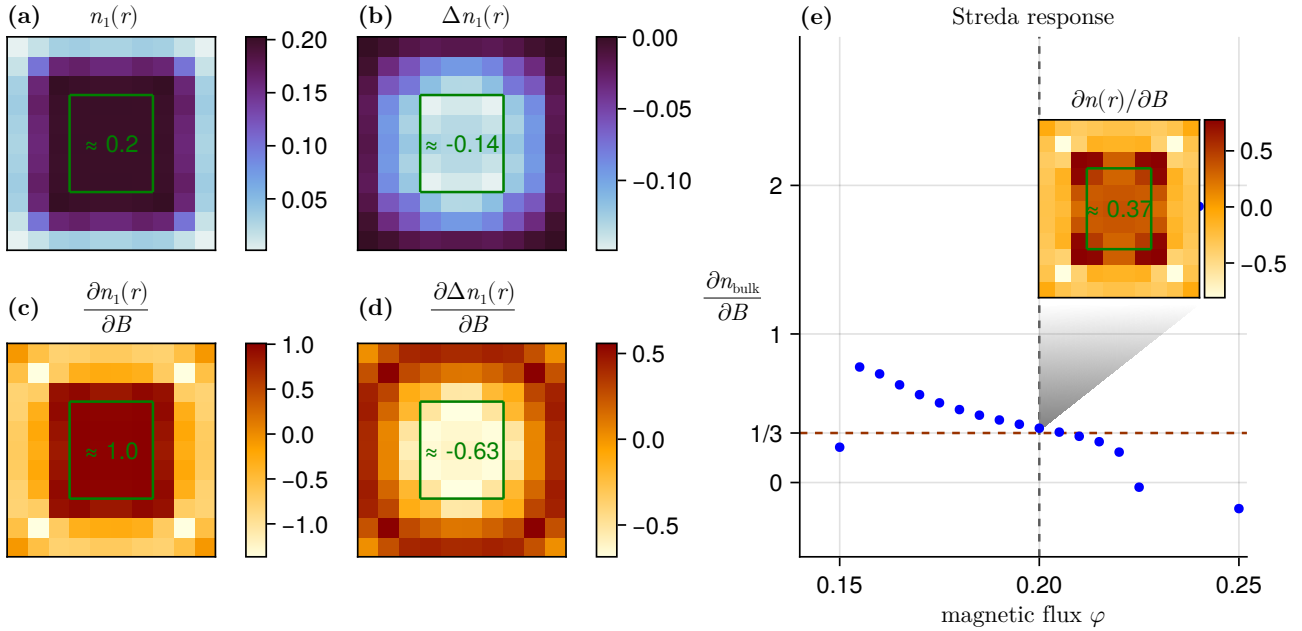


FIG. 4. **Středa-response and Luttinger's theorem violation in the FCI state.** (a,b) Spatial distributions of the local Luttinger count $n_1(\mathbf{r})$ and Luttinger integral $\Delta n_1(\mathbf{r})$, defined in Eq. (11). The presence of a finite, negative $\Delta n_1(\mathbf{r})$ in the bulk directly signals the breakdown of Luttinger's theorem. (c,d) Středa responses of the Luttinger count and the Luttinger integral densities. The derivative of n_1 with respect to magnetic field (averaged over the bulk sites enclosed by the green contour) yields an integer-valued response, corresponding to an Ishikawa-Matsuyama invariant $N_3[G] \simeq 1$. By contrast, the Středa response of Δn_1 is fractional and accounts for the difference between $N_3[G]$ and the many-body Chern number. (e) Středa response of the total bulk electron density as a function of magnetic flux per plaquette. The developing plateau near $1/3$ is consistent with the fractional Hall conductance of the FCI state realized at flux $\varphi = 1/5$. The inset shows the spatially-resolved magnetic response of the total density $n(\mathbf{r})$ at $\varphi = 1/5$.

the torus and the box results can be expected to disappear in the thermodynamical limit (see Section B).

The main panel in Fig. 3(b) shows the momentum-resolved spectral densities $A(k, \omega) = -\frac{1}{\pi} \text{Im} [G(k, \omega + i0^+)]$ and $S(k, \omega) = -\frac{1}{\pi} \text{Im} [\Sigma(k, \omega + i0^+)]$, plotted as a function of the real frequency ω and magnetic crystal momentum k on the torus geometry. The Green's function is obtained from a thermodynamic average over the three-fold ground-state manifold $\{|\Psi_0^j\rangle, j = 1, 2, 3\}$, such that

$$A(k, \omega) = \frac{1}{3} \sum_{j=1}^3 \sum_n [|\langle \Psi_0^j | \hat{c}_k | \Psi_n \rangle|^2 \delta(\omega - E_n + E_0) + |\langle \Psi_0^j | \hat{c}_k^\dagger | \Psi_n \rangle|^2 \delta(\omega + E_n - E_0)], \quad (13)$$

with $|\Psi_n^j\rangle$ the eigenstates of the Hamiltonian in the $N \pm 1$ particle sector and E_n their corresponding eigenvalues. Both spectral functions display only a weak dependence on momentum. We note that in the continuum FQH limit, the Green's function is expected to be strictly momentum independent [60, 61]. This striking feature of the Green's functions results from the homogeneity of the FQH liquid and the flatness of the Landau levels [61]. Accordingly, the residual momentum dependence reflects the finite dispersion of the LHB at flux $\varphi = 1/5$ and is expected to diminish as

the system approaches the continuum limit. The role of the ground-state averaging is illustrated in the inset of Fig. 3(b), which shows the spectral densities obtained by restricting the averaging to a single ground-state $|\Psi_0^1\rangle$:

$$\tilde{A}(k, \omega) = \sum_n [|\langle \Psi_0^1 | \hat{c}_k | \Psi_n \rangle|^2 \delta(\omega - E_n + E_0) + |\langle \Psi_0^1 | \hat{c}_k^\dagger | \Psi_n \rangle|^2 \delta(\omega + E_n - E_0)]. \quad (14)$$

In this case, a pronounced momentum dependent structure appears in the positions of the poles of both $\tilde{S}(k, \omega)$ and $\tilde{A}(k, \omega)$, repeated with period $2\pi/N_x \cdot 3$. This periodicity can be naturally traced back to the different sets of momenta available for the excited states in the thin-torus limit [62, 63]. While the actual eigenstates in two-dimensions are different from those in the quasi-one dimensional limit, this characteristic momentum periodicity is expected to persist for any finite circumference of the torus. A more detailed discussion of this behavior is provided in Section C. Our results are consistent with the momentum dependence of the local density-of-states reported in the thin cylinder limit in a recent preprint [12].

B. Numerical Study of Green's Function Topological Invariants

Having characterized the poles and zeros of the Green's function along the real-frequency axis, we now turn to the central result of this work: a direct numerical evaluation of Green's function topological invariants in a fractional Chern insulator. Specifically, we compute the densities of the Luttinger count $n_1(\mathbf{r})$ and the Luttinger integral $\Delta n_1(\mathbf{r})$, together with their magnetic-field responses, by numerically performing the contour integration in the complex frequency plane prescribed by Eq. (11). This procedure provides an explicit, non-perturbative determination of $N_1[G]$ and ΔN_1 , and their Středa responses, $N_3[G]$ and ΔN_3 , in a strongly correlated, topologically ordered state. The calculations are carried out in the box geometry, allowing direct access to the bulk Green's functions.

The position of the chemical potential within the charge gap, relative to the zero of the Green's function, determines the value of the Luttinger count, as anticipated in the general overview of Section II. Topological insulators are special in this respect: In contrast to a topologically trivial insulator – where the chemical potential can be fixed by simply taking the zero-temperature limit [46] – a topological insulator with open boundaries responds differently: shifting the chemical potential alters the occupation of the conducting edge states and thus represents a physically meaningful operation, one that can be tuned experimentally through electrostatic gating. In this section, we fix the chemical potential between the main electron-removal peak and the in-gap self-energy pole. This choice allows us to evaluate the Luttinger count and integral directly from the ED data while avoiding spurious finite-size effects. For other choices of μ , the contour integration in the complex frequency plane becomes more sensitive to finite-size edge contributions, as discussed in detail in Section A 2. The integration can however be performed when the finite-size effects stemming from the edge poles of the Green's functions are eliminated by hand. We follow that route in Section V.

The spatial distributions of Luttinger count density $n_1(\mathbf{r})$ and the Luttinger integral density $\Delta n_1(\mathbf{r})$ are shown in Fig. 4 (a) and (b), respectively. Both quantities exhibit well-defined plateaus in the bulk of the system, indicating that finite-size and boundary effects are well controlled. Their bulk-averaged values unambiguously reveal a violation of Luttinger's theorem in the FCI state. The bulk value of the Luttinger count, $n_1 \simeq 0.2$, corresponds to a completely filled LHB, since the magnetic unit cell contains five lattice sites. This value of the Luttinger count is in agreement with the analytical structure of the Green's function shown in Fig. 3, where a single pole appears below the chosen chemical potential for each LHB state. By construction, the Luttinger count assigns unit weight to each such pole, thereby overestimating the physical particle density, as anticipated in Section II. The Luttinger integral Δn_1 must therefore be negative, compensating for the difference between the actual spectral weight of the hole peak and unity, as illustrated in Fig. 2 (b).

The Středa responses of the local electronic density $n(\mathbf{r})$

and of its constituents, the Luttinger count $n_1(\mathbf{r})$ and the Luttinger integral densities $\Delta n_1(\mathbf{r})$, are shown in Figs. 4 (c–e). Resolving the total density response of individual Luttinger components reveals a striking separation of integer and fractional contributions. The bulk Středa response of the Luttinger count, $\partial n_1/\partial B$, displayed in Fig. 4(c), yields a quantized value $N_3[G] \simeq 1$, indicating that the Ishikawa-Matsuyama invariant remains strictly integer in an FCI state in spite of the fractional value of the many-body Chern number. In contrast, the fractional Hall response is entirely captured by the Středa response of the Luttinger integral, $\partial \Delta n_1/\partial B \simeq -2/3$, shown in Fig. 4(d). The associated invariant ΔN_3 precisely accounts for the difference between $N_3[G]$ and the fractional many-body Chern number $C_{\text{MB}} = 1/3$, consistent with the theoretical predictions of Ref. [27]. The many-body Chern number is directly reflected in the Středa response of the total bulk density, shown in Fig. 4(e) as a function of the flux per plaquette φ , where a clear developing plateau near $1/3$ emerges around $\varphi = 1/5$.

Our results appear to contradict previous analytical predictions for the value of $N_3[G]$ in FQH states [24], where a μ -independent value of $N_3[G]=3$ was inferred for the $\nu=1/3$ Laughlin state by evaluating a momentum-resolved Luttinger count. Importantly, that previous approach used the low-energy form of the electron edge Green's function [31] and invoked the bulk-edge correspondence proven in Ref. [30]. We argue that this discrepancy arises because the “edge winding number” entering the bulk-edge correspondence in Ref. [30] is defined in terms of the full electron edge Green's function over all frequencies, whereas the low-energy edge theory constrains only its behavior arbitrarily close to the chemical potential. In an FCI state, the electron edge Green's function generically contains non-universal high-energy structure that is invisible to the low-energy theory but can nevertheless contribute to the Green's function winding. We therefore conjecture that reconstructing $N_3[G]$ from the low-energy electron edge data alone is not generically valid in fractionalized phases.

Summarizing, our numerical studies demonstrate that the Ishikawa-Matsuyama invariant takes the value $N_3[G]=1$ deep in the bulk of a Laughlin-type FCI state, for a given choice of the chemical potential in the gap. In the following Section, we will analytically demonstrate that this topological invariant is fully determined by the Luttinger count N_1 together with the single-particle Chern number of the occupied Bloch band, provided interaction-induced Bloch-band mixing is neglected.

IV. ANALYTICAL EVALUATION OF $N_3[G]$ IN THE ABSENCE OF BLOCH BAND MIXING

To clarify the origin of the numerical observations above and their deviation from the predictions of Ref. [24], we analytically evaluate the Green's function winding number $N_3[G]$ in the limit where Bloch band mixing can be neglected. By this we mean that, throughout the frequency range relevant for determining $N_3[G]$, the interacting Green's function is well approximated as diagonal in the band index.

This approximation is justified whenever the interaction scale is small compared to the energy gaps separating different Bloch bands, so that interaction-induced virtual transitions into other bands only weakly affect the Green's function in the frequency range relevant for the contour integration defining the invariant. It is also exact whenever the many-body Hamiltonian has been explicitly projected onto a chosen band, in which case band mixing is absent by construction, as in Eq. (10).

We begin by expressing the interacting one-body Green's function in the basis of single-particle magnetic Bloch orbitals $|u_{\alpha\mathbf{k}}\rangle = \hat{c}_{\alpha\mathbf{k}}^\dagger|0\rangle$. Magnetic translation symmetry implies that crystal momentum remains a good quantum number, so that the Green's function decomposes into independent \mathbf{k} sectors. Within each sector, and assuming the propagator is diagonal in the band index, we may write

$$\hat{G}_{\mathbf{k}}(z) = \sum_{\alpha} g_{\alpha\mathbf{k}}(z) |u_{\alpha\mathbf{k}}\rangle\langle u_{\alpha\mathbf{k}}|. \quad (15)$$

Here we represent the Green's function as an operator acting on the single-particle Hilbert space spanned by the magnetic Bloch orbitals. This makes the momentum derivatives appearing in Eq. (1) explicit, since they act both on the scalar functions $g_{\alpha\mathbf{k}}(z)$ and on the \mathbf{k} -dependence of the basis states. Alternatively, one may introduce a \mathbf{k} -independent reference basis $\{|n\rangle\}$ and express the propagator in matrix form,

$$G_{\mathbf{k}}(z) = U_{\mathbf{k}} g_{\mathbf{k}}(z) U_{\mathbf{k}}^\dagger, \quad (16)$$

where $g_{\mathbf{k}}(z) = \text{diag}(g_{\alpha\mathbf{k}}(z))$ and $U_{\mathbf{k}}^{n\alpha} = \langle n|u_{\alpha\mathbf{k}}\rangle$ is a unitary transformation encoding the \mathbf{k} -dependence of the Bloch basis.

At zero temperature, the scalar functions $g_{\alpha\mathbf{k}}(z)$ entering Eq. (15) are defined as

$$g_{\alpha\mathbf{k}}(z) = -\frac{1}{d_g} \sum_{j=1}^{d_g} \int_0^\infty d\tau e^{z\tau} \langle \Psi_0^j | \mathcal{T}_\tau \hat{c}_{\alpha\mathbf{k}}(\tau) \hat{c}_{\alpha\mathbf{k}}^\dagger(0) | \Psi_0^j \rangle, \quad (17)$$

where \mathcal{T}_τ denotes imaginary-time ordering and $|\Psi_0^j\rangle$ are the d_g (topologically) degenerate many-body ground states. This expression corresponds to the zero-temperature limit of the finite-temperature Green's function in the presence of ground-state degeneracy, resulting in a statistical average over the degenerate manifold.

Substituting Eq. (15) (or equivalently the matrix representation in Eq. (16)) into the definition of the topological invariant Eq. (1), and using the fact that the diagonal elements $g_{\alpha\mathbf{k}}(z)$ possess a meromorphic structure in frequency (Eq. (5)), one may perform the frequency integration explicitly, see Section D for details. Assuming that no poles nor zeros of the propagator cross the chemical potential, one obtains

$$N_3[G] = \frac{1}{2\pi} \sum_{\alpha} \int d^2k \mathcal{F}_{xy}^{\alpha}(\mathbf{k}) \times \left(\sum_p \Theta(\mu - \varepsilon_{\alpha\mathbf{k}}^{(p)}) - \sum_s \Theta(\mu - \chi_{\alpha\mathbf{k}}^{(s)}) \right), \quad (18)$$

where $\mathcal{F}_{xy}^{\alpha}(\mathbf{k}) = i(\langle \partial_{k_x} u_{\alpha\mathbf{k}} | \partial_{k_y} u_{\alpha\mathbf{k}} \rangle - \langle \partial_{k_y} u_{\alpha\mathbf{k}} | \partial_{k_x} u_{\alpha\mathbf{k}} \rangle)$ is the Berry curvature of the α -th magnetic Bloch band, and $\varepsilon_{n\mathbf{k}}^{(p)}$ and $\chi_{n\mathbf{k}}^{(s)}$ denote the poles and zeros of the corresponding scalar Green's function. Interestingly, Eq. (18) mirrors the spirit of Ref. [64], which proposed that the Hall conductivity of an interacting system might be captured by integrating the single-particle Berry curvature weighted by suitably defined occupation factors. Subsequent work [65, 66] showed that such one-body expressions fail to reproduce the true many-body Hall response in generic interacting topological phases. This is fully consistent with $N_3[G]$ reflecting the topology of the single-particle Green's function rather than the many-body Chern number.

If the number of poles and zeros lying below the chemical potential for each band α is independent of crystal momentum, as in Fig. 3(b), Eq. (18) further reduces to

$$N_3[G] = \frac{A_{\text{cell}}}{A} \sum_{\alpha} N_1[G_{\alpha}] C_{\alpha}, \quad (19)$$

where A_{cell} is the area of the magnetic unit cell, A is the total area of the system, C_{α} is the Chern number of the α -th magnetic Bloch band, and

$$N_1[G_{\alpha}] = A \int \frac{d^2k}{(2\pi)^2} \left(\sum_p \Theta(\mu - \varepsilon_{\alpha\mathbf{k}}^{(p)}) - \sum_s \Theta(\mu - \chi_{\alpha\mathbf{k}}^{(s)}) \right) \quad (20)$$

counts the net number of occupied poles minus zeros associated with band α . Equation (19) is fully consistent with the numerical results obtained in the previous section from evaluating $N_3[G]$ via the magnetic-field derivative of the bulk Luttinger count in a box geometry. In particular, when partially filling the lowest Hofstadter band (with Chern number $C_0 = 1$), we found $N_1[G_0]/A \approx 0.2$ at the chosen chemical potential. Since $A_{\text{cell}} = 5$, Eq. (19) yields the prediction $N_3 \approx 1$, in excellent agreement with our numerical evaluation.

Moreover, the results in Eqs. (19) and (20) predict a change in the value of $N_3[G]$ as the chemical potential shifts to the right with respect to the in-gap Green's functions zero shown in Fig. 3. In that case, the Luttinger count is expected to vanish, since the contribution from each pole below the Fermi level is canceled by a zero. This change in the Luttinger count leads to the vanishing of the Ishikawa-Matsuyama invariant $N_3[G]=0$ in that case, according to Eq. (19).

Before concluding this section, we note that Eq. (19) becomes even simpler in the continuum Landau-level limit. In this case, the interacting Green's function within a fixed Landau level is independent of crystal momentum, $g_{\alpha\mathbf{k}}(z) \equiv g_{\alpha}(z)$, so all poles and zeros associated with that Landau level are dispersionless. Each Landau level carries Chern number $C_{\alpha} = 1$, and the magnetic unit cell has area $A_{\text{cell}} = \Phi_0/B$. Since the total flux is $\Phi = BA$, Eq. (19) reduces to

$$N_3[G] = \frac{\Phi_0}{\Phi} N_1[G]. \quad (21)$$

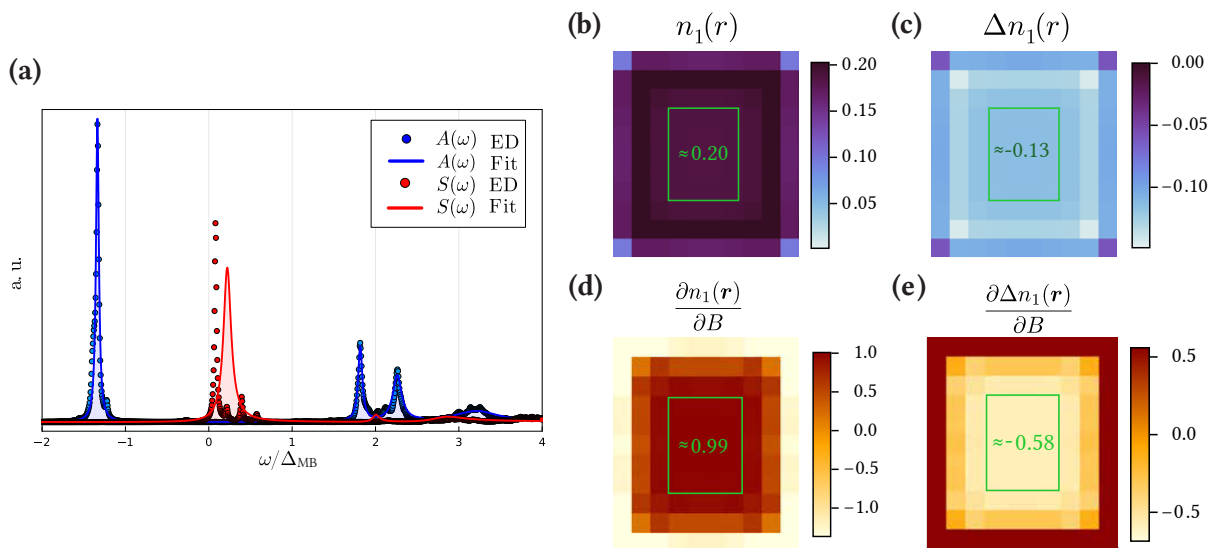


FIG. 5. Extraction of the self-energy, the Luttinger count and the Luttinger integral from the spectral functions obtained with ED. **(a)** The spectral densities A and S defined in Eq. (12) as obtained from the exact diagonalization and extracted from the model Eq. (26). Note, that $A(\omega)$ and $S(\omega)$ are plotted in different scales. **(b)** and **(c)** The distribution of the localized versions of the Luttinger count n_1 and the Luttinger integral Δn_1 over the lattice, as defined in Eq. (11). **(c)** The Středa response of the Luttinger count n_1 and the Luttinger integral Δn_1 densities. The bulk value of the approximate $\frac{\partial n_1}{\partial B}$ allows us to estimate the Ishikawa-Matsuyama invariant by $N_3 = 0.99 \pm 0.01$ in agreement with our numerical Fig. 4 and analytical results Section IV. **(d)** The fractional valued Středa response of the Luttinger integral $\Delta N_3 = -0.58 \pm 0.02$ as before balances the difference between the many-body Chern number and N_3 .

Introducing the Luttinger-count density $n_1 = N_1[G]/A$ and considering that $\partial N_3[G]/\partial B = 0$, we obtain from Eq. (21) the relation

$$N_3[G] = \Phi_0 \left. \frac{\partial n_1}{\partial B} \right|_{\mu}, \quad (22)$$

consistent with Ref. [27].

V. EXTRACTING $N_3[G]$ AND ΔN_3 FROM THE LOCAL DENSITY OF STATES

Let us discuss how our predictions can be tested experimentally. In this section we propose a scheme for extracting the Luttinger count, integral and their Středa responses directly from the LDOS probes, which were obtained recently for FCI states [13, 14]. The values of $N_3[G]$ and $\Delta N_3[G]$ are the functionals of the Green's functions, self-energy and their derivatives with respect to magnetic field. In general, extracting the Green's functions and the self-energy from the local density of states is a challenging, if not impossible task [67–69]. For a Laughlin-type FCI state the scheme significantly simplifies as will be clarified below. We outline the protocol, and then, as a proof of concept, we extract $N_3[G]$ and $\Delta N_3[G]$ from the local density of states that were obtained numerically.

The scheme exploits several characteristic features of the Laughlin-type FCI's Green's functions. In the continuum LL limit, the spatial and temporal dependencies of the

Green's functions are disentangled due to their momentum independence. This limit is well realized for the parameters used in Fig. 3. In this regime, the frequency dependence of the Green's functions is fully determined by the local density of states, while the spatial dependence of the Green's functions is governed solely by the non-interacting single-particle density matrix. Consequently, the Green's functions projected onto the LHB assume the form of Eq. (15), with a momentum independent function g :

$$\hat{G}_{\mathbf{k}}(z) = g(z) |u_{\mathbf{k}}\rangle \langle u_{\mathbf{k}}|. \quad (23)$$

Here we dropped the band index α , neglecting the mixing with the higher Hofstadter bands. The spectral functions provide us with the imaginary part of the function $g(\omega)$. The real part can be obtained from the Kramers-Kronig relations. Thus, the Green's functions $G(r, r; z)$ can be obtained, provided that the non-interacting Bloch vectors $|u_{\mathbf{k}}\rangle$ are known.

An additional simplification stems from the observation that the spectral function of the Laughlin-type FCI's is composed of a small number of sharp coherent peaks well separated from the incoherent background; see Fig. 3 and Refs [6, 8]. This motivates a simple model for the spectral functions consisting of a sum of a few narrow Lorentzians, representing the coherent part of the spectrum and an additional broader Lorentzian peak representing the

incoherent background:

$$A_{\text{fit}}(\omega) = A_{\text{coh}}(\omega) + A_{\text{inc}}(\omega), \quad (24)$$

$$A_{\text{coh}}(\omega) = \sum_{k=1}^{N_p} Z_k \frac{\gamma_k^2}{(\omega - \omega_k)^2 + \gamma_k^2}, \quad (25)$$

$$A_{\text{inc}}(\omega) = Z_b \frac{\Gamma^2}{(\omega - \Omega)^2 + \Gamma^2}. \quad (26)$$

Here N_p is the number of coherent peaks, Z_k are the spectral weights of the coherent peaks, ω_k and γ_k are their positions and widths; Ω and Γ represent the position and width of the incoherent peaks, respectively. Fitting the spectral functions with $A_{\text{fit}}(\omega)$, one readily obtains the approximate frequency dependent part of the Green's functions:

$$g_{\text{fit}}(\omega) = \sum_{k=1}^{N_p} \frac{\pi Z_k \gamma_k}{\omega - \omega_k + i\gamma_k} + \frac{\pi Z_b \Gamma}{\omega - \Omega + i\Gamma}. \quad (27)$$

We now apply the procedure to the spectral functions that were numerically obtained for the $\nu = \frac{1}{3}$ FCI state; see Fig. 3. For this state we observed the three dominant coherent peaks $N_p = 3$, one corresponding to the hole-like state, and the other two corresponding to the particle-like side of the spectrum. We fitted the data with the model spectral functions in Eq. (26). Since we are ultimately interested in the response of the particle density to a small perturbing magnetic field, we included in the minimization procedure a Lagrange multiplier penalizing the deviation of the area under the peaks from the area under the data peaks. Once the approximate $g_{\text{fit}}(\omega)$ are obtained, the Green's functions can be calculated from Eq. (23). Thereafter, we evaluate numerically the derivatives of the Green's functions and the self-energy with respect to magnetic field, repeating the protocol for the spectral functions of the same system in a small perturbing magnetic field. Finally we evaluate the local densities of the Luttinger count, the Luttinger integral Eq. (11) and the corresponding Středa responses.

The resulting approximate spectral functions $A_{\text{fit}}(\omega)$ and $S_{\text{fit}}(\omega)$ Eq. (12) along with the distributions of the Luttinger count $n_1(\mathbf{r})$, the Luttinger integral $\Delta n_1(r)$ and their derivatives with respect to the magnetic field are presented in Fig. 5. The approximate and the exact results presented in Figs. 5 and 4 respectively are in a remarkable agreement, given the simplicity of the model Green's functions. The self-energy peak $S_{\text{fit}}(\omega)$ in the many-body gap presented in panel (a) of Fig. 5 deviates only slightly from the exact result. The situation can be further improved by a more adequate model for the incoherent part of the spectral function A_{inc} . We found that, while the position of the peak is quite robust to the fine details of the model for A_{inc} , the position does depend on the spectral weight Z_b of the background. The bulk values of the approximate Luttinger count $n_1 = 0.2000 \pm 0.0001$, and the Luttinger integral $\delta n_1 = 0.131 \pm 0.002$ are in a good agreement with the ED results Fig. 4 and the theoretical predictions.

Most importantly, the protocol allowed us to estimate the values of the Ishikawa-Matsuyama invariant $N_3[G]$ and the correction $\Delta N_3[G]$ from the local density of states, which can be directly accessed experimentally. For the same choice

of the chemical potential as in Section III B we obtain $N_3 = 0.99 \pm 0.01$ and $\Delta N_3 = -0.58 \pm 0.02$ in agreement with the ED results, whereas for the complex integration contour enclosing the bulk zero $N_3 = 0.001 \pm 0.009$ and $\Delta N_3 = -0.39 \pm 0.02$. Let us note that the experimental data for the spectral functions $A(\omega)$ reported in [13, 14] exhibit a more complicated structure than the ED results used in our tests. A convolution with the DOS of the tip obscures the sharp coherent picture among other factors inherent to a real experiment. Nevertheless, this proof-of-concept implementation of the protocol gives us a ground for a cautious optimism regarding the experimental assessment of our results.

VI. CONCLUDING REMARKS

In this work we investigated single-particle Green's functions and their associated topological invariants, the Luttinger count and Ishikawa-Matsuyama invariant, for a Laughlin-type FCI state. By explicitly evaluating the Luttinger count and the Luttinger integral [2], we demonstrated the breakdown of Luttinger's theorem. Using the connection between Green's function invariants and Středa responses [27], we evaluated $N_3[G]$ and its deviation from the many-body Chern number, $\Delta N_3[G]$, as the magnetic responses of the Luttinger count and the Luttinger integral, respectively. We found that the fractional nature of the Středa response, characteristic of FCI states, is entirely captured by the response of the Luttinger integral, while $N_3[G]$ itself encodes only the single-particle topology inherited from the underlying magnetic Bloch bands and the momentum resolved values of the Luttinger count. Finally, we proposed a scheme directly relating the experimentally accessible local density of states [13, 14] to the Luttinger count, integral and their corresponding Středa responses $N_3[G]$ and $\Delta N_3[G]$.

Our results raise several intriguing directions for future work. One appealing scenario is an interface between two FCI states with different quantized values of the Ishikawa-Matsuyama invariant. According to the bulk-boundary correspondence of Ref. [23], the mismatch in N_3 should be reflected in the Luttinger count of the boundary Green's function, so that dispersive branches of zeros or poles of the boundary Green's functions are expected to emerge and cross the chemical potential. An especially interesting case occurs when two FCI states share the same many-body Chern number but differ in their Ishikawa-Matsuyama invariant due to a shift in the chemical potential. Even if the boundary remains gapped, the analytical structure of the boundary Green's functions is expected to undergo qualitative changes [23], pointing toward interfacial phenomena beyond those captured by conventional many-body topology [70].

Addressing these questions may require complementary numerical and analytical methods. Tensor-network methods [71, 72], which have already proven effective for FCI studies [73–85], could be adapted with controlled accuracy [86] through benchmarking against exact diagonalization. Diagrammatic Monte-Carlo methods [87]

have recently revealed signatures of FQH physics in the Green's functions [88], while analytical approaches based on composite-fermion theories [9] or the thin torus limit [12] may further elucidate the single-electron structure of fractionalized topological matter.

Acknowledgments The authors warmly thank Antoine Georges for his insightful feedback on the manuscript and for discussions. They also acknowledge discussions with Victor Gurarie, Matteo Rizzi, Laurens Vanderstraeten and Botao Wang. This research was partly financially supported by the ERC Grant LATIS, the FRS-FNRS (Belgium), the EOS project CHEQS, and the Fondation ULB. A.A.M and A.M.N also acknowledge the financial support from the Russian Quantum Center in the framework of the Russian Quantum Technologies Roadmap. L.P.G. acknowledges support provided by the FRS-FNRS Belgium and the L'Oréal-UNESCO for Women in Science Programme.

Contribution statement A.A.M. conceived the project with inputs from L.P.G., N.G and A.M.N. The numerical simulations were performed and lead by A.M.N, with contributions from A.A.M. The analytical calculations were performed by L.P.G. and N.R.C. All authors analyzed and discussed the results. A.A.M., L.P.G., N.G. and A.M.N. wrote the manuscript with inputs from N.R.C. The research was supervised by L.P.G., N.G. and A.A.M.

Appendix A: Numerical Evaluation of the Relevant Quantities

1. Green's functions and self-energy

In this appendix we present details of the numerical evaluation of the Green's functions for the FCI state. The numerical calculation of the derivatives of the Luttinger count and the Luttinger integral Eq. (11) with respect to the magnetic field requires working with open boundary conditions. This is a consequence of the Dirac quantization of the magnetic field under periodic boundary conditions, which does not allow for infinitesimally small variations of the magnetic field for a finite system. The extraction of bulk Green's functions under open boundary conditions is possible only when the system size is large compared to the correlation length. To make the calculations feasible, we therefore consider the Harper–Hofstadter–Hubbard model projected onto the lowest Hofstadter band Eq. (10).

We start by diagonalizing the non-interacting Hofstadter Hamiltonian for a given geometry:

$$\begin{aligned} H_0 &= \sum_{n,m} -t (c_{n,m+1}^\dagger c_{n,m} + c_{n+1,m}^\dagger c_{n,m} e^{i2\pi m\varphi} + h.c.) \\ &\equiv \sum_{ij} h_{ij} c_i^\dagger c_j = \sum_{\beta=1}^{N_s} \varepsilon_\beta c_\beta^\dagger c_\beta, \end{aligned} \quad (\text{A1})$$

where N_s is the number of sites and the operators c_j and c_β are related by $c_j = \sum_\beta U_{j,\beta} c_\beta$ with $U_{j,\beta}$ being the matrix

of eigenvectors of the single-particle Hamiltonian h_{ij} . The nearest-neighbor Hubbard interaction

$$H_{int} = \sum_{\langle ij \rangle} V : n_i n_j : \quad (\text{A2})$$

can then be expressed in terms of the operators c_β . The normally ordered projected Hamiltonian in Eq. (10) is obtained by truncating the sums over β , keeping only the operators corresponding to the lowest Hofstadter band. The resulting Hamiltonian in the Fock space generated by the operators c_β is then constructed and diagonalized numerically using the Lanczos algorithm [89]. In our implementation, we employ the Arpack.jl Julia package, which provides a Julia wrapper around the Fortran ARPACK library.

The Green's functions are evaluated numerically using the Lehmann representation [90], which at zero temperature reads

$$\begin{aligned} G_{\gamma,\beta}(z) &= \sum_m \frac{\langle 0 | c_\gamma | m^{N+1} \rangle \langle m^{N+1} | c_\beta^\dagger | 0 \rangle}{z - (E_m^{N+1} - E_0)} \\ &+ \sum_m \frac{\langle 0 | c_\beta^\dagger | m^{N-1} \rangle \langle m^{N-1} | c_\gamma | 0 \rangle}{z + (E_m^{N-1} - E_0)}. \end{aligned} \quad (\text{A3})$$

Here $|m^{N\pm 1}\rangle$ and $E_m^{N\pm 1}$ denote the eigenstates and eigenvalues of the Hamiltonian Eq. (10) for $N \pm 1$ particles. The procedure starts by obtaining the ground-state vector $|0\rangle$ for a fixed number of particles N , after which the states $c_\beta^{(\dagger)} |0\rangle$ are constructed. The key step in the Lanczos-based numerical evaluation of the Green's functions is the approximation of the resolvent operator $\frac{1}{z\mathbb{1} - \hat{H}}$ by its projection onto the Krylov space $\frac{1}{z\mathbb{1} - \hat{H}}$ [91]. If the Krylov space \mathcal{K} has dimensionality $M_{\mathcal{K}}$, the Krylov projected operator $\frac{1}{z\mathbb{1} - \hat{H}}$ reproduces the same first $2M_{\mathcal{K}} + 1$ moments $\int d\omega G_{\beta\beta}(\omega) \omega^m$ of the exact operator $\frac{1}{z\mathbb{1} - \hat{H}}$ [91]. Therefore, although the Lanczos algorithm does not provide accurate approximations for the highly excited states $|m^{N\pm 1}\rangle$, the Green's functions obtained in this way converge rapidly to the exact ones as $M_{\mathcal{K}}$ increases.

Once the Green's functions are obtained in the eigenbasis of the Harper-Hofstadter Hamiltonian, the self-energy is computed using the Dyson equation: $G(z)^{-1} = G_0^{-1}(z) - \Sigma(z)$. Importantly, the order of matrix-inversion and the transformation to the real-space basis matters. The self-energy must first be evaluated in the eigenbasis of the Harper-Hofstadter Hamiltonian and only afterwards transformed to the real-space basis. This is due to the mismatch between the sizes of the two bases arising from the projection onto the lowest Hofstadter band. In particular, the Green's function expressed in the real-space basis has rank equal only to the number of states in the LHB, making its inversion ill-defined.

2. Evaluation of $n_1(r)$ and $\Delta n_1(r)$.

We next compute the localized versions of the Luttinger count and the Luttinger integral, defined in Eq. (11), and evaluate their numerical derivative with respect to magnetic field. Here we summarize the procedure used in the calculations.

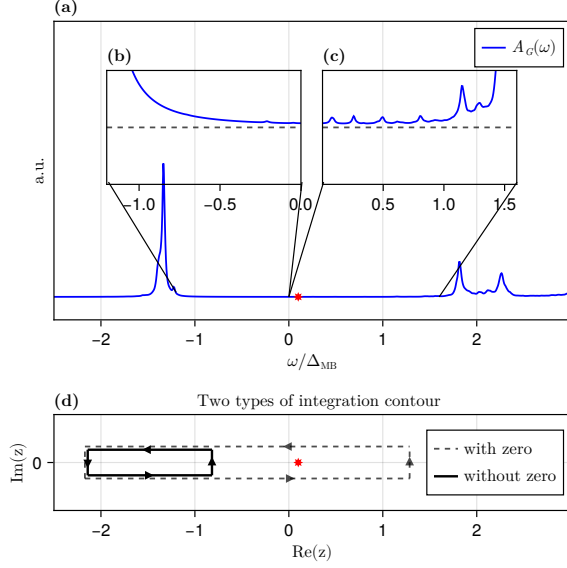


FIG. 6. **(a)** Local density of states in the bulk. Insets **(b,c)** show the density of states on a smaller scale below and above $\omega = 0$, respectively. **(d)** Schematic illustration of the possible integration contours for evaluating the local Luttinger count and the Luttinger integral, Eq. (11). The red star indicates the position of the in-gap bulk Green's function zero. Because edge-induced poles of the Green's function appear above $\omega = 0$, the numerical integration is performed only along the contour shown in solid line.

The integration contour over continuous Matsubara frequencies appearing in the definitions of the Luttinger count and the Luttinger integral (Eq. (4c)) can be closed in the lower half of the complex-frequency plane. The contour can then be deformed into the shape presented schematically in Fig. 6 (d). During this deformation, no Green's function pole or zero should cross the contour, as doing so would make the integrand in Eq. (11) singular and prevent convergence. As discussed in the main text, the chemical potential can be chosen arbitrarily within the charge gap. Depending on this choice, the single zero of the bulk Green's function lies either within or outside the integration contour. In practice, stable numerical convergence is achieved only for contours that do not enclose the zero. The convergence crucially depends on the regularity of the Green's functions and self-energies close to the points where the contour crosses the real-frequency axis. As demonstrated in Fig. 6 (a-c) the spectral density develops additional peaks inside the charge gap to the right of the bulk Green's function zero. These additional peaks are absent in the spectral densities in periodic boundary conditions and can be attributed to in-gap edge contributions to the density of states, as detailed in Appendix B.

Appendix B: Finite-Size Effects

Throughout the work we aim to characterize the bulk properties of the FQH droplet. The finite size of our system

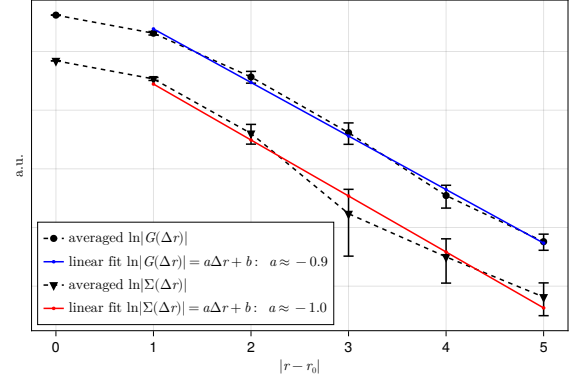


FIG. 7. **Spatial decay of the Green's function and self-energy.** Dashed curve with circle (triangle) markers shows the Green's function (self-energy) behavior averaged over different paths from the bulk region toward the edge. The data are shown on a logarithmic y -axis. Solid lines indicate linear fits yielding a correlation length of $l_{\text{cor}} \sim 1$ lattice constant.

affects the results in two distinct ways. First, under open boundary conditions, edge and bulk physics may mix due to the finite spatial extent of the system. Second, the limited size can modify the bulk properties themselves. The latter effect is present even in calculations performed with periodic boundary conditions. To quantify both types of finite-size effects, we begin by analyzing the decay of correlation functions.

Correlation functions in the bulk of the FCI state decay at least exponentially fast[100], since all bulk excitations are gapped. Figure 7 shows the spatial decay of the Green's functions and self-energies at zero frequency on a logarithmic scale. The linear fits (solid lines) demonstrate that the Green's functions can be bounded by $G(r, r'; \omega) < e^{-|r-r'|/l_{\text{cor}}}$ with a correlation length of the order of one lattice constant, $l_{\text{cor}} \approx 1$. That this bound applies at arbitrary frequency follows from the decomposition in Eq. (23), which states that the temporal and spatial dependencies of the Green's functions factorize with a good accuracy for an almost flat LHB. Another immediate consequence of the decomposition in Eq. (23) is that the decay of Green's functions is determined by the noninteracting Hamiltonian. The obtained correlation length $l_{\text{cor}} \approx 1$ is compatible with the magnetic length at the flux $\varphi = \frac{1}{5}$: $l_B = \sqrt{\frac{q}{2\pi}} \approx 0.9$.

Let us first discuss the finite-size effects arising from the influence of the metallic edges. As anticipated in the previous section, in-gap poles of the Green's functions associated with the edges affect the convergence of the numerical evaluation of n_1 , Δn_1 , and their Středa responses. The convergence of the integration relies on the regularity of the integrand in Eq. (11). In particular, no poles or zeros of the Green's functions matrix elements $G(r, r'; \omega)$ should appear in the vicinity of the points where the integration contour intersects the real-frequency axis. As demonstrated in Fig. 8, this condition is not satisfied for contours enclosing the single bulk Green's function zero.

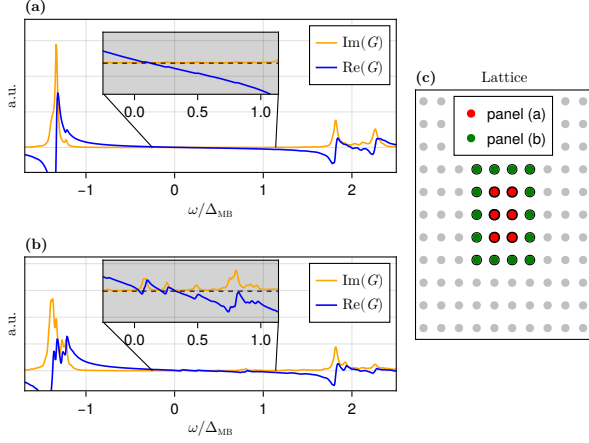


FIG. 8. Illustration of the influence of edge-induced poles and zeros of the Green's function on the numerical evaluation of n_1 and Δn_1 . (a) Real and imaginary parts of the diagonal elements of the Green's functions in the center of the sample, highlighted in red in panel (c). (b) Real and imaginary parts of the diagonal Green's function averaged over the region highlighted in green in panel (c), where multiple poles and zeros appear.

This zero, located within the single-particle gap, is visible in Fig. 8(a) as the point where both the real and imaginary parts of the Green's function $G(r_0, r_0; \omega)$ vanish for any site r_0 within the central red region in Fig. 8(c). However, moving just one lattice site toward the edge (green region in Fig. 8(c)) and averaging over this larger region already reveals additional poles and zeros. Despite the short correlation length of order one lattice constant these additional divergencies spoil the convergence of the numerical integration for contours enclosing the bulk zero. In practice, we therefore restrict the integration to contours that cross the real axis below the bulk zero, ensuring stable evaluation of the Luttinger count and the Luttinger integral.

The second type of finite-size arises from the limited system size itself, which modifies the bulk properties even in the absence of edges, as realized on the torus. In particular, the spectral densities shown in Fig. 3(a) obtained with periodic (torus) and open (box) boundary conditions are visibly different. The double-peak structure on the particle side of the spectral functions, predicted in Ref. [8], is evident in the box geometry, whereas on the torus each peak appears to be split into several smaller peaks. We argue that the general structure of the spectral functions on torus becomes compatible with the one obtained in the bulk of the box geometry as the system size increases. To support this, we computed the spectral densities on the torus for larger systems with a fixed particle number $N = 6$. The resulting densities of states are presented in Fig. 9, where the characteristic double-peak structure followed by an incoherent background emerges clearly for larger system sizes, matching the bulk behavior seen in the box geometry.

Let us close the section by discussing finite-size effects on the Středa response in the FQH state. Figure 4 panel (e) of the

main text shows the onset of the plateau in the Středa response $\frac{\partial n}{\partial B}$ as a function of the magnetic flux per unit cell, near the chosen value $\varphi = 1/5$. We verified that the plateau stabilizes in a larger system of 15×15 sites, as shown in Fig. 10. Since the exact number of bulk states in the LHB cannot be determined precisely in the box geometry, we computed the response using both 15 and 18 states in the LHB and observe that a clear plateau emerges in both cases.

Appendix C: Momentum Dependence of Ground State Correlators on a Torus

As demonstrated in the inset of Fig. 3(b), the spectral functions $\tilde{A}(k, \omega)$ calculated by choosing a single ground state:

$$\tilde{A}(k, \omega) = \sum_n [|\langle \Psi_0^1 | \hat{c}_k | \Psi_n \rangle|^2 \delta(\omega - E_n + E_0) + |\langle \Psi_0^1 | \hat{c}_k^\dagger | \Psi_n \rangle|^2 \delta(\omega + E_n - E_0)], \quad (C1)$$

feature a momentum dependence that is absent for the thermodynamically averaged spectral functions $A(k, \omega)$ Eq. (12). There is a clear periodic structure in the positions of the Green's functions zeros and poles with a period $2\pi/N_x \cdot 3$. In this section we argue that this peculiar momentum dependence arises naturally in the thin torus limit [62, 63, 93, 94] and persists — albeit gradually disappearing — as the torus circumference increases.

FQH states in the continuum can be adiabatically connected to Tao-Thouless crystal states [12, 62, 63, 93, 94]. Remarkably, these crystalline states are exact solutions of the problem of a partially filled Landau level in the thin-torus or cylinder limit. Let us outline the main steps of the procedure. Consider a $2d$ electronic system in a uniform magnetic field B in the Landau gauge $\mathbf{A} = -(By, 0)$ on a torus. We assume that the torus is infinite in the y -direction $L_y \rightarrow \infty$ and finite in the explicitly translationally invariant x -direction. The single-electron wave functions in the lowest Landau level are plane waves in the x -direction and Gaussian localized in the y -direction:

$$\psi_k(x, y) \sim e^{ikx} \exp\left[-\frac{1}{2\ell_B^2} (y - k\ell_B^2)^2\right]. \quad (C2)$$

Here $\ell_B = \sqrt{\frac{\hbar c}{eB}}$ is the magnetic length. The centers of localization of the states $\psi_k(x, y)$ are equally spaced in y -direction with a spacing $2\pi\ell_B^2/L_x$.

A general density-density interaction projected onto the lowest Landau level takes the form[63]:

$$\hat{H}_{int} = \sum_{\{k_i\}} V_{k_1, k_2, k_3, k_4} c_{k_1}^\dagger c_{k_2}^\dagger c_{k_3} c_{k_4}, \quad (C3)$$

$$V_{k_1, k_2, k_3, k_4} = \int d^2\mathbf{r}_1 d^2\mathbf{r}_2 \psi_{k_1}^*(\mathbf{r}_1) \psi_{k_2}^*(\mathbf{r}_2) \times V(|\mathbf{r}_1 - \mathbf{r}_2|) \psi_{k_3}(\mathbf{r}_2) \psi_{k_4}(\mathbf{r}_1).$$

In the limit $L_x/\ell_B \rightarrow 0$ the overlap between the wavefunctions $\psi_{k_1}(x, y)$ and $\psi_{k_2}(x, y)$ becomes exponentially small. As

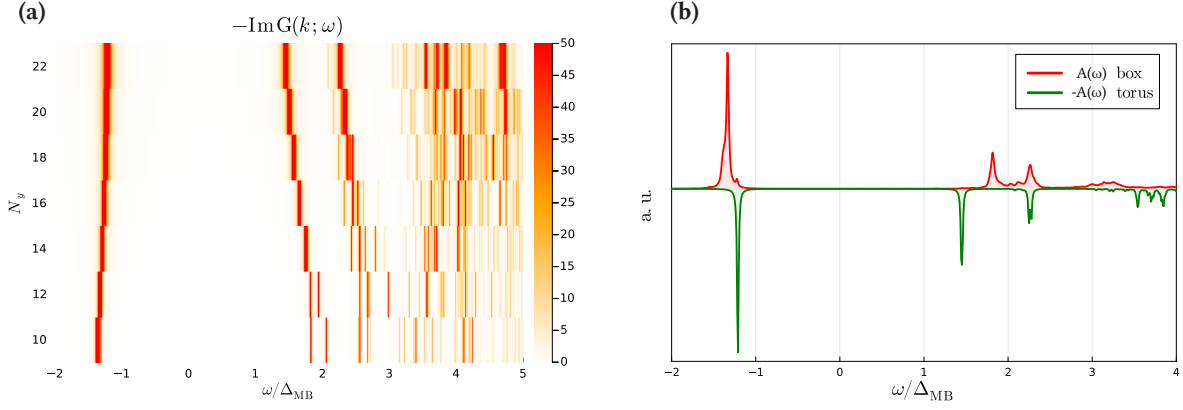


FIG. 9. (a) Spectral densities $A(\omega)$ for different system sizes, obtained by increasing N_y while keeping $N_x = 9$ constant. The number of particles is fixed to $N = 6$, while the magnetic flux per plaquette is $\varphi = 1/q$ with $q = N_y/2$, ensuring a constant filling fraction of $\nu = 1/3$. (b) Comparison between the spectral densities $A(\omega)$ for a torus of size $N_y = 22$, $N_x = 9$ and for a box with $N_y = 11$, $N_x = 10$.

a result, the only surviving terms in Eq. (C3) correspond to simple electrostatic repulsion between the fermions on a quasi-one-dimensional lattice. Since the Landau level is flat, the Hamiltonian in this limit reduces to

$$\hat{H}_{TT} = \sum_{i,k} V_k n_i n_{i+k}. \quad (\text{C4})$$

At a filling fraction $\nu = 1/(2m + 1)$ the energy is minimized by a crystalline state in which the fermions are separated from

each other as far as possible. At the filling $\nu = 1/3$ the ground states in the occupation basis are:

$$|\Psi_0^1\rangle = |\dots 001001001\dots\rangle. \quad (\text{C5})$$

The three degenerate ground states are related to each other by translations of this pattern and therefore carry different total momenta. The equal-time correlators $\langle \Psi_0^1 | c_k^\dagger c_k | \Psi_0^1 \rangle$ are therefore momentum-dependent and exhibit a $\frac{2\pi}{L_x} \cdot 3$ periodicity. Outside the strict Tao–Thouless limit $L_x/\ell_B \rightarrow 0$, the scattering between states with different k cannot be neglected and the density starts to fluctuate. However, the modulation of the occupation of the momentum states $\langle \Psi_0^1 | c_k^\dagger c_k | \Psi_0^1 \rangle$ persists at any finite L_x .

The Laughlin-type FCI states exhibit essentially the same physics [95]. Fig. 11 (a) shows the momentum-state occupations for a single ground state and different values of the magnetic flux per plaquette $\varphi = 1/q$ in a torus with dimensions $N_y = 2q$, $N_x = 9$ and a fixed number of particles $N = 6$. Increasing the value of q increases the magnetic length and therefore brings the system closer to the thin torus limit. As a result, the modulation of the momentum-states occupation becomes more pronounced with increasing q and persists up to $q = 5$, corresponding to the results presented in the main text. The momentum dependence of the spectral densities $\tilde{A}(\omega, \mathbf{k})$ and $\tilde{S}(\omega, \mathbf{k})$ becomes respectively more pronounced for larger q as illustrated in Fig. 11 (b).

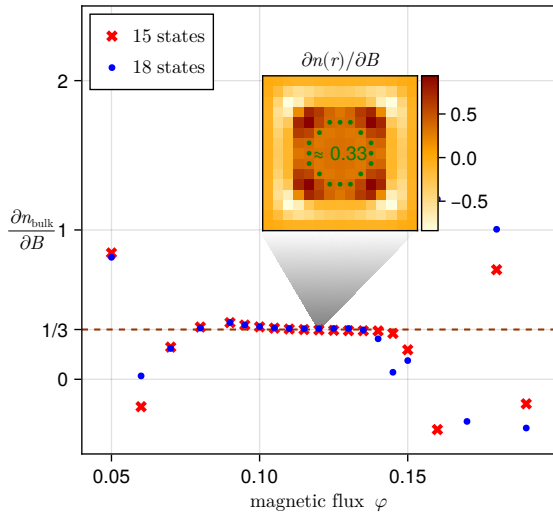


FIG. 10. Stabilization of the Středa response in a larger system with 15×15 sites and 6 particles. The many-body Chern number extracted from the Středa response as a function of the magnetic flux per unit cell exhibits a clear plateau corresponding to the $1/3$ FCI in the range $0.08 < \varphi < 0.14$ (in units of the flux quantum Φ_0). The inset shows the spatially resolved density response, yielding a bulk Chern number of $C_{MB} = 0.33 \pm 0.01$. Red crosses and blue circles correspond to calculations with different number of bulk states retained in the LHB projection.

Appendix D: Derivation of Eq. (18)

We present here additional details on the derivation of Eq. (18) in the main text, which provides a simplified expression for the Ishikawa-Matsuyama invariant when the single-particle Green's function is approximated as diagonal in the Bloch band index. Substituting Eq. (15) into Eq. (1),

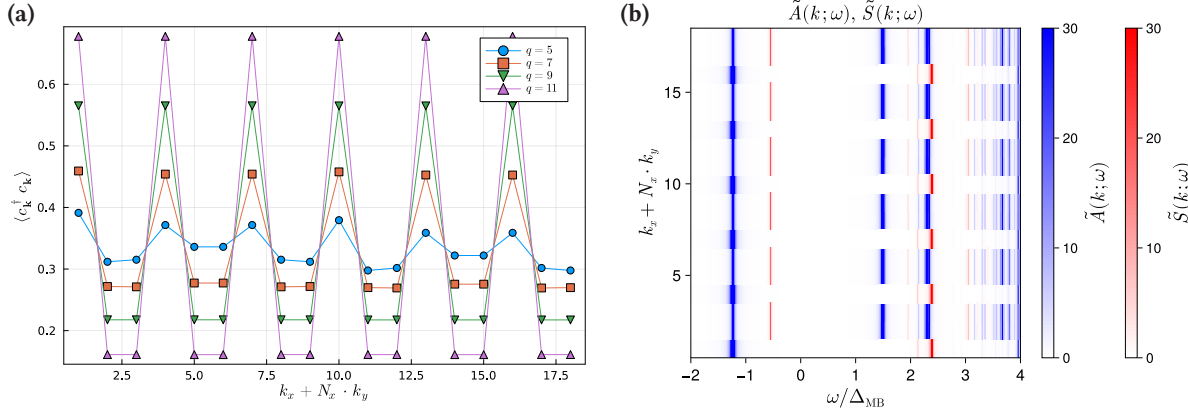


FIG. 11. **(a)** Momentum-state occupations $\langle \Psi_0^\dagger | c_k^\dagger c_k | \Psi_0 \rangle$ for one of the degenerate ground states $|\Psi_0\rangle$ on the torus for different values of the magnetic flux per unit cell $\varphi = 1/q$. The torus has dimensions $N_y = 2q$ and fixed $N_x = 9$. Increasing q increases the magnetic length ℓ_B , bringing the system closer to the thin-torus limit. **(b)** Spectral functions of the Green's function, $\tilde{A}(\omega, \mathbf{k})$, and of the self-energy, $\tilde{S}(\omega, \mathbf{k})$, defined in Eq. (C1), shown for $q = 11$.

and after some algebra, one obtains

$$N_3[G] = -\frac{\epsilon^{0\nu\rho}}{8\pi^2} \sum_\alpha \int dz e^{z0^+} \int d^2k \left[2g_{\alpha\mathbf{k}}^{-1} \frac{\partial g_{\alpha\mathbf{k}}}{\partial z} \langle \partial_{k_\nu} u_{\alpha\mathbf{k}} | \partial_{k_\rho} u_{\alpha\mathbf{k}} \rangle - \sum_\beta \left(\frac{\partial g_{\alpha\mathbf{k}}}{\partial z} g_{\beta\mathbf{k}}^{-1} - \frac{\partial g_{\alpha\mathbf{k}}^{-1}}{\partial z} g_{\beta\mathbf{k}} \right) \langle \partial_{k_\nu} u_{\alpha\mathbf{k}} | u_{\beta\mathbf{k}} \rangle \langle u_{\beta\mathbf{k}} | \partial_{k_\rho} u_{\alpha\mathbf{k}} \rangle \right], \quad (\text{D1})$$

where summation over repeated indices ν, ρ is implicit. The frequency integral in the first term of Eq. (D1) can be evaluated explicitly using the meromorphic structure of the diagonal Green's function elements,

$$g_{\alpha\mathbf{k}}(z) = \frac{\prod_s (z - \chi_{\alpha\mathbf{k}}^{(s)})}{\prod_p (z - \varepsilon_{\alpha\mathbf{k}}^{(p)})}, \quad (\text{D2})$$

where $\varepsilon_{\alpha\mathbf{k}}^{(p)}$ denotes their poles and $\chi_{\alpha\mathbf{k}}^{(s)}$ their zeros. Using Eq. (D2), one readily finds

$$\int dz e^{z0^+} g_{\alpha\mathbf{k}}^{-1}(z) \frac{\partial g_{\alpha\mathbf{k}}}{\partial z} = \int dz e^{z0^+} \left(\sum_s \frac{1}{z - \chi_{\alpha\mathbf{k}}^{(s)}} - \sum_p \frac{1}{z - \varepsilon_{\alpha\mathbf{k}}^{(p)}} \right) = 2\pi i \left(\sum_s \Theta(\mu - \chi_{\alpha\mathbf{k}}^{(s)}) - \sum_p \Theta(\mu - \varepsilon_{\alpha\mathbf{k}}^{(p)}) \right), \quad (\text{D3})$$

where we have used that the contour integration in the complex frequency plane selects the residues of poles and zeros lying below the chemical potential μ . After performing an integration by parts in the last term of Eq. (D1) and

inserting Eq. (D3), one arrives at

$$N_3[G] = \sum_\alpha \int \frac{d^2k}{2\pi} \mathcal{F}_{xy}^\alpha(\mathbf{k}) \left(\sum_p \Theta(\mu - \varepsilon_{\alpha\mathbf{k}}^{(p)}) - \sum_s \Theta(\mu - \chi_{\alpha\mathbf{k}}^{(s)}) \right) + \frac{\epsilon^{0\nu\rho}}{8\pi^2} \sum_{\alpha\beta} \int d^2k \mathcal{B}_{\alpha\beta}(\mathbf{k}, \mu) \langle \partial_{k_\nu} u_{\alpha\mathbf{k}} | u_{\beta\mathbf{k}} \rangle \langle u_{\beta\mathbf{k}} | \partial_{k_\rho} u_{\alpha\mathbf{k}} \rangle, \quad (\text{D4})$$

with

$$\mathcal{F}_{xy}^\alpha(\mathbf{k}) = i(\langle \partial_{k_x} u_{\alpha\mathbf{k}} | \partial_{k_y} u_{\alpha\mathbf{k}} \rangle - \langle \partial_{k_y} u_{\alpha\mathbf{k}} | \partial_{k_x} u_{\alpha\mathbf{k}} \rangle) \quad (\text{D5})$$

the Berry curvature of the α -th Bloch band and

$$\mathcal{B}_{\alpha\beta}(\mathbf{k}, \mu) = \int dz e^{z0^+} \frac{\partial}{\partial z} (g_{\alpha\mathbf{k}} g_{\beta\mathbf{k}}^{-1}) = -2i \text{Im} [g_{\alpha\mathbf{k}}(\mu + i0^+) g_{\beta\mathbf{k}}^{-1}(\mu + i0^+)] \quad (\text{D6})$$

an on-shell (boundary) term that only depends on the properties of the Green's function at the chemical potential. If there are no poles nor zeros at μ , this term vanishes identically and Eq. (D4) reduces to Eq. (18) in the main text.

As a sanity check, one can evaluate Eq. (D4) in the non-interacting limit, where $\hat{G}_\mathbf{k}(z) = (z - \hat{H}_\mathbf{k})^{-1}$, with $\hat{H}_\mathbf{k}$ the single-particle Bloch Hamiltonian. In this case, $g_{\alpha\mathbf{k}}(z) = 1/(z - \varepsilon_{\alpha\mathbf{k}})$, with $\varepsilon_{\alpha\mathbf{k}}$ the energy of the Bloch band corresponding to the eigenstate $|u_{\alpha\mathbf{k}}\rangle$. The boundary contribution in Eq. (D6) then evaluates to

$$\mathcal{B}_{\alpha\beta}(\mathbf{k}, \mu) = -2\pi i (\varepsilon_{\mathbf{k}\beta} - \varepsilon_{\mathbf{k}\alpha}) \delta(\varepsilon_{\mathbf{k}\alpha} - \mu), \quad (\text{D7})$$

and Eq. (D4) reduces to

$$N_3[G] = \frac{1}{2\pi} \sum_\alpha \int d^2k \mathcal{F}_{xy}^\alpha(\mathbf{k}) \Theta(\mu - \varepsilon_{\alpha\mathbf{k}}) + \frac{\Phi_0}{(2\pi)^2} \sum_\alpha \int d^2k m_z^\alpha(\mathbf{k}) \delta(\varepsilon_{\alpha\mathbf{k}} - \mu), \quad (\text{D8})$$

where

$$m_z^\alpha(\mathbf{k}) = \frac{2\pi}{\Phi_0} \text{Im} \left[\langle \partial_{k_x} u_{\alpha\mathbf{k}} | \hat{H}_{\mathbf{k}} - \varepsilon_{\alpha\mathbf{k}} | \partial_{k_y} u_{\alpha\mathbf{k}} \rangle \right] \quad (\text{D9})$$

is the intrinsic orbital magnetic moment of the α -th Bloch

eigenstate. This reproduces the known Štředa response of non-interacting Bloch electrons [96, 97], for which $N_3[G] = \Phi_0 \partial n / \partial B$ at fixed chemical potential and zero temperature, explicitly given by Eq. (D8).

-
- [1] Evgenii Mikhailovich Lifshitz and Lev Petrovich Pitaevskii. *Statistical physics: theory of the condensed state*, volume 9. Elsevier, 2013.
- [2] Joaquin Mazdak Luttinger and John Clive Ward. Ground-state energy of a many-fermion system. ii. *Physical Review*, 118(5):1417, 1960.
- [3] Daniel C Tsui, Horst L Stormer, and Arthur C Gossard. Two-dimensional magnetotransport in the extreme quantum limit. *Physical Review Letters*, 48(22):1559, 1982.
- [4] Siddharth A Parameswaran, Rahul Roy, and Shivaji L Sondhi. Fractional quantum Hall physics in topological flat bands. *Comptes Rendus Physique*, 14(9-10):816–839, 2013.
- [5] Robert B Laughlin. Anomalous quantum hall effect: An incompressible quantum fluid with fractionally charged excitations. *Physical Review Letters*, 50(18):1395, 1983.
- [6] EH Rezayi. Electron and quasiparticle density of states in the fractionally quantized Hall effect. *Physical Review B*, 35(6):3032, 1987.
- [7] Song He, PM Platzman, and BI Halperin. Tunneling into a two-dimensional electron system in a strong magnetic field. *Physical review letters*, 71(5):777, 1993.
- [8] Jainendra K. Jain and Michael R. Peterson. Reconstructing the Electron in a Fractionalized Quantum Fluid. *Phys. Rev. Lett.*, 94:186808, May 2005.
- [9] Xinlei Yue and Ady Stern. Electronic excitations in the bulk of fractional quantum Hall states. *Physical Review B*, 110(11):115428, 2024.
- [10] Mytraya Gattu and JK Jain. Unlocking new regimes in fractional quantum Hall effect with quaternions. *Physical Review Letters*, 134(15):156501, 2025.
- [11] Fabian Pichler, Wilhelm Kadow, Clemens Kuhlenkamp, and Michael Knap. Single-particle spectral function of fractional quantum anomalous Hall states. *Physical Review B*, 111(7):075108, 2025.
- [12] Jyesta M Adhidewata and Joel E Moore. Excitation and tunneling spectra of a fractional quantum Hall system in the thin cylinder limit. *arXiv preprint arXiv:2507.21375*, 2025.
- [13] Gelareh Farahi, Cheng-Li Chiu, Xiaomeng Liu, Zlatko Papić, Kenji Watanabe, Takashi Taniguchi, Michael P Zaletel, and Ali Yazdani. Broken symmetries and excitation spectra of interacting electrons in partially filled Landau levels. *Nature Physics*, 19(10):1482–1488, 2023.
- [14] Yuwen Hu, Yen-Chen Tsui, Minhao He, Umut Kamber, Taige Wang, Amir S Mohammadi, Kenji Watanabe, Takashi Taniguchi, Zlatko Papić, Michael P Zaletel, et al. High-resolution tunnelling spectroscopy of fractional quantum Hall states. *Nature Physics*, pages 1–8, 2025.
- [15] Kenzo Ishikawa and Toyoki Matsuyama. Magnetic field induced multi-component QED3 and quantum Hall effect. *Zeitschrift für Physik C Particles and Fields*, 33(1):41–45, 1986.
- [16] Grigory E Volovik. *The universe in a helium droplet*, volume 117. Oxford University Press on Demand, 2003.
- [17] Grigory E Volovik. Quantum phase transitions from topology in momentum space. In *Quantum analogues: from phase transitions to black holes and cosmology*, pages 31–73. Springer, 2007.
- [18] John Clive Ward. An identity in quantum electrodynamics. *Physical Review*, 78(2):182, 1950.
- [19] Yasushi Takahashi. On the generalized ward identity. *Il Nuovo Cimento (1955-1965)*, 6(2):371–375, 1957.
- [20] Qian Niu and DJ Thouless. Quantised adiabatic charge transport in the presence of substrate disorder and many-body interaction. *Journal of Physics A: Mathematical and General*, 17(12):2453, 1984.
- [21] Joseph E Avron and Ruedi Seiler. Quantization of the Hall conductance for general, multiparticle Schrödinger Hamiltonians. *Physical review letters*, 54(4):259, 1985.
- [22] Xi Wu and MA Zubkov. Anomalous fractional quantum hall effect and multi-valued hamiltonians. *Journal of Physics: Condensed Matter*, 33(35):355601, 2021.
- [23] Victor Gurarie. Single-particle Green’s functions and interacting topological insulators. *Physical Review B*, 83(8):085426, 2011.
- [24] Victor Gurarie and Andrew M Essin. Topological invariants for fractional quantum Hall states. *JETP letters*, 97(4):233–238, 2013.
- [25] Yuan-Yao He, Han-Qing Wu, Zi Yang Meng, and Zhong-Yi Lu. Topological invariants for interacting topological insulators. II. Breakdown of single-particle Green’s function formalism. *Physical Review B*, 93(19):195164, 2016.
- [26] Jinchao Zhao, Peizhi Mai, Barry Bradlyn, and Philip Phillips. Failure of topological invariants in strongly correlated matter. *Physical review letters*, 131(10):106601, 2023.
- [27] Lucila Peralta Gavensky, Subir Sachdev, and Nathan Goldman. Connecting the many-body Chern number to Luttinger’s theorem through Štředa’s formula. *Physical review letters*, 131(23):236601, 2023.
- [28] Andrea Blason and Michele Fabrizio. Unified role of Green’s function poles and zeros in correlated topological insulators. *Physical Review B*, 108(12):125115, 2023.
- [29] Steffen Bollmann, Chandan Setty, Urban FP Seifert, and Elio J König. Topological Green’s function zeros in an exactly solved model and beyond. *Physical Review Letters*, 133(13):136504, 2024.
- [30] Andrew M. Essin and Victor Gurarie. Bulk-boundary correspondence of topological insulators from their respective Green’s functions. *Phys. Rev. B*, 84:125132, Sep 2011.
- [31] Xiao-Gang Wen. Chiral Luttinger liquid and the edge excitations in the fractional quantum Hall states. *Physical Review B*, 41(18):12838, 1990.
- [32] V Gurarie. Topological invariant for the orbital spin of the electrons in the quantum Hall regime and Hall viscosity. *Journal of Physics: Condensed Matter*, 27(7):075601, 2015.
- [33] A Widom. Thermodynamic derivation of the Hall effect current. *Physics Letters A*, 90(9):474, 1982.
- [34] P Štředa. Theory of quantised Hall conductivity in two dimensions. *Journal of Physics C: Solid State Physics*,

- 15(22):L717, 1982.
- [35] This equality holds only in the absence of poles and zeros of the Green's function at the chemical potential; see [27] for details.
- [36] Andrey V Cnubukov, Dirk K Morr, and Konstantin A Shakhnovich. Fermi surface evolution in underdoped cuprates. *Philosophical Magazine B*, 74(5):563–571, 1996.
- [37] Andrey V Chubukov and Dirk K Morr. Electronic structure of underdoped cuprates. *Physics Reports*, 288(1-6):355–387, 1997.
- [38] BL Altshuler, AV Chubukov, A Dashevskii, AM Finkel' Stein, and DK Morr. Luttinger theorem for a spin-density-wave state. *Europhysics Letters*, 41(4):401, 1998.
- [39] Antoine Georges, Olivier Parcollet, and Subir Sachdev. Quantum fluctuations of a nearly critical Heisenberg spin glass. *Physical Review B*, 63(13):134406, 2001.
- [40] A Rosch. Breakdown of Luttinger's theorem in two-orbital Mott insulators. *The European Physical Journal B*, 59(4):495–502, 2007.
- [41] Joshua T Heath and Kevin S Bedell. Necessary and sufficient conditions for the validity of Luttinger's theorem. *New Journal of Physics*, 22(6):063011, 2020.
- [42] R. Žitko, G. G. Blesio, L. O. Manuel, and A. A. Aligia. Iron phthalocyanine on Au(111) is a “non-Landau” Fermi liquid. *Nature Communications*, 12(1):6027, 2021.
- [43] Jan Skolimowski and Michele Fabrizio. Luttinger's theorem in the presence of Luttinger surfaces. *Physical Review B*, 106(4):045109, 2022.
- [44] Chandan Setty, Fang Xie, Shouvik Sur, Lei Chen, Maia G Vergniory, and Qimiao Si. Electronic properties, correlated topology, and Green's function zeros. *Physical Review Research*, 6(3):033235, 2024.
- [45] Behnam Farid and Alexei M Tselik. Comment on “Breakdown of the Luttinger sum rule within the Mott-Hubbard insulator”, by J. Kokalj and P. Prelovsek [Phys. Rev. B 78, 153103 (2008), arXiv: arXiv: 0803.4468]. *arXiv preprint arXiv:0909.2886*, 2009.
- [46] Behnam Farid. Comment on “Absence of Luttinger's Theorem”, by Kiaran B. Dave, Philip W. Phillips and Charles L. Kane, arXiv: 1207.4201. *arXiv preprint arXiv:1211.5612*, 2012.
- [47] Tudor D Stanescu and Gabriel Kotliar. Fermi arcs and hidden zeros of the green function in the pseudogap state. *Physical Review B—Condensed Matter and Materials Physics*, 74(12):125110, 2006.
- [48] Tudor D Stanescu, Philip Phillips, and Ting-Pong Choy. Theory of the Luttinger surface in doped Mott insulators. *Physical Review B—Condensed Matter and Materials Physics*, 75(10):104503, 2007.
- [49] Kiaran B Dave, Philip W Phillips, and Charles L Kane. Absence of Luttinger's theorem due to zeros in the single-particle green function. *Physical review letters*, 110(9):090403, 2013.
- [50] Mathias S Scheurer, Shubhayu Chatterjee, Wei Wu, Michel Ferrero, Antoine Georges, and Subir Sachdev. Topological order in the pseudogap metal. *Proceedings of the National Academy of Sciences*, 115(16):E3665–E3672, 2018.
- [51] Fenner Harper. *The Hofstadter model and other fractional chern insulators*. PhD thesis, University of Oxford, 2015.
- [52] Felix Alexander Palm. *Fractional chern insulators in Hofstadter-Hubbard models*. PhD thesis, lmu, 2023.
- [53] Kazuhiro Seki and Seiji Yunoki. Topological interpretation of the Luttinger theorem. *Physical Review B*, 96(8):085124, 2017.
- [54] Thomas Scaffidi and Gunnar Möller. Adiabatic continuation of fractional Chern insulators to fractional quantum Hall states. *Physical review letters*, 109(24):246805, 2012.
- [55] The explicit lattice translational symmetry is broken in the presence of the homogeneous magnetic field. All the gauge invariant quantities, however have to preserve the translational symmetry. The elements of the Green's functions and the self-energy which are diagonal in space indices are gauge invariant and therefore are translational invariant [?].
- [56] E. H. Rezayi. Electron and quasiparticle density of states in the fractionally quantized Hall effect. *Phys. Rev. B*, 35:3032–3035, Feb 1987.
- [57] Giovanni Vignale. Integral charge quasiparticles in a fractional quantum Hall liquid. *Phys. Rev. B*, 73:073306, Feb 2006.
- [58] Mytraya Gattu, G. J. Sreejith, and J. K. Jain. Scanning tunneling microscopy of fractional quantum Hall states: Spectroscopy of composite-fermion bound states. *Phys. Rev. B*, 109:L201123, May 2024.
- [59] SM Girvin. Particle-hole symmetry in the anomalous quantum Hall effect. *Physical Review B*, 29(10):6012, 1984.
- [60] Rudolf Haussmann, Hiroyuki Mori, and AH MacDonald. Correlation energy and tunneling density of states in the fractional quantum Hall regime. *Physical review letters*, 76(6):979, 1996.
- [61] Benjamin Currie. Non-Fermi liquid physics in the lowest Landau level: A diagrammatic expansion approach.
- [62] R Tao and DJ Thouless. Fractional quantization of Hall conductance. *Physical Review B*, 28(2):1142, 1983.
- [63] EJ Bergholtz and Anders Karlhede. Quantum hall system in tao-thouless limit. *Physical Review B—Condensed Matter and Materials Physics*, 77(15):155308, 2008.
- [64] Titus Neupert, Luiz Santos, Claudio Chamon, and Christopher Mudry. Elementary formula for the Hall conductivity of interacting systems. *Phys. Rev. B*, 86:165133, Oct 2012.
- [65] Steven H. Simon, Fenner Harper, and N. Read. Comment on “Elementary formula for the Hall conductivity of interacting systems”. *Phys. Rev. B*, 89:127101, Mar 2014.
- [66] Titus Neupert, Luiz Santos, Claudio Chamon, and Christopher Mudry. Reply to “Comment on ‘Elementary formula for the Hall conductivity of interacting systems’ ”. *Phys. Rev. B*, 89:127102, Mar 2014.
- [67] T Valla, AV Fedorov, PD Johnson, BO Wells, SL Hulbert, Qiang Li, GD Gu, and N Koshizuka. Evidence for quantum critical behavior in the optimally doped cuprate $\text{Bi}_2\text{Sr}_2\text{CaCu}_2\text{O}_{8+\delta}$. *Science*, 285(5436):2110–2113, 1999.
- [68] Joonho Jang, Heun Mo Yoo, LN Pfeiffer, KW West, KW Baldwin, and Raymond C Ashoori. Full momentum-and energy-resolved spectral function of a 2D electronic system. *Science*, 358(6365):901–906, 2017.
- [69] B Sriram Shastry. Method for reconstructing the self-energy from the spectral function. *Physical Review B*, 110(15):155149, 2024.
- [70] Niklas Wagner, Lorenzo Crippa, Adriano Amaricci, Philipp Hansmann, Marcel Klett, EJ König, Thomas Schäfer, D Di Sante, Jennifer Cano, AJ Millis, et al. Mott insulators with boundary zeros. *Nature Communications*, 14(1):7531, 2023.
- [71] Steven R White. Density matrix formulation for quantum renormalization groups. *Physical review letters*, 69(19):2863, 1992.
- [72] Jacob Jordan, Roman Orús, Guifre Vidal, Frank Verstraete, and J Ignacio Cirac. Classical simulation of infinite-size quantum lattice systems in two spatial dimensions. *Physical review letters*, 101(25):250602, 2008.
- [73] AE Feiguin, E Rezayi, C Nayak, and S Das Sarma.

- Density matrix renormalization group study of incompressible fractional quantum hall states. *Physical review letters*, 100(16):166803, 2008.
- [74] A. G. Grushin, J. Motruk, M. P. Zaletel, and F. Pollmann. Characterization and stability of a fermionic $\nu = 1/3$ fractional Chern insulator. *Phys. Rev. B*, 91:035136, 2015.
- [75] J. Motruk, A. G. Grushin, F. de Juan, and F. Pollmann. Interaction-driven phases in the half-filled honeycomb lattice: An infinite density matrix renormalization group study. *Phys. Rev. B*, 92:085147, 2015.
- [76] Y.-C. He, F. Grusdt, A. Kaufman, M. Greiner, and A. Vishwanath. Realizing and adiabatically preparing bosonic integer and fractional quantum Hall states in optical lattices. *Phys. Rev. B*, 96:201103, 2017.
- [77] J. Motruk and F. Pollmann. Phase transitions and adiabatic preparation of a fractional Chern insulator in a boson cold-atom model. *Phys. Rev. B*, 96:165107, 2017.
- [78] X.-Y. Dong, A. G. Grushin, J. Motruk, and F. Pollmann. Charge excitation dynamics in bosonic fractional Chern insulators. *Phys. Rev. Lett.*, 121:086401, 2018.
- [79] P. Rosson, M. Lubasch, M. Kiffner, and D. Jaksch. Bosonic fractional quantum Hall states on a finite cylinder. *Phys. Rev. A*, 99:033603, 2019.
- [80] L. Schoonderwoerd, F. Pollmann, and G. Möller. Interaction-driven plateau transition between integer and fractional Chern insulators. *arXiv*, 2019.
- [81] F. A. Palm, M. Buser, J. Léonard, M. Aidelsburger, U. Schollwöck, and F. Grusdt. Bosonic Pfaffian state in the Hofstadter-Bose-Hubbard model. *Phys. Rev. B*, 103:L161101, 2021.
- [82] B. Andrews, T. Neupert, and G. Möller. Stability, phase transitions, and numerical breakdown of fractional Chern insulators in higher Chern bands of the Hofstadter model. *Phys. Rev. B*, 104:125107, 2021.
- [83] J. Boesl, R. Dilip, F. Pollmann, and M. Knap. Characterizing fractional topological phases of lattice bosons near the first Mott lobe. *Phys. Rev. B*, 105:075135, 2022.
- [84] E. L. Weerda and M. Rizzi. Fractional quantum Hall states with variational projected entangled-pair states: A study of the bosonic Harper-Hofstadter model. *Phys. Rev. B*, 109:L241117, 2024.
- [85] Chloé Van Bastelaere, Felix A Palm, Botao Wang, Nathan Goldman, and Laurens Vanderstraeten. Fractional quantum hall wedding cakes. *arXiv preprint arXiv:2510.15472*, 2025.
- [86] Min Long, Hongyu Lu, Han-Qing Wu, and Zi Yang Meng. Spectra of magnetoroton and chiral graviton modes of fractional chern insulator. *arXiv preprint arXiv:2501.00247*, 2024.
- [87] Nikolai V Prokof'ev and Boris V Svistunov. Polaron problem by diagrammatic quantum monte carlo. *Physical review letters*, 81(12):2514, 1998.
- [88] Ben Currie and Evgeny Kozik. Fractional quantum hall states by feynman's diagrammatic expansion. *arXiv preprint arXiv:2412.21064*, 2024.
- [89] Cornelius Lanczos. An iteration method for the solution of the eigenvalue problem of linear differential and integral operators. *Journal of research of the National Bureau of Standards*, 45(4):255–282, 1950.
- [90] Alexander Altland and Ben D Simons. *Condensed matter field theory*. Cambridge university press, 2010.
- [91] Erik Koch. 8 The Lanczos Method. *The LDA+ DMFT approach to strongly correlated materials*, 2011.
- [92] In fact, for a Laughlin-type FCI state one may expect correlations to decay faster than exponentially.
- [93] Alexander Seidel, Henry Fu, Dung-Hai Lee, Jon Magne Leinaas, and Joel Moore. Incompressible quantum liquids and new conservation laws. *Physical review letters*, 95(26):266405, 2005.
- [94] Emil J Bergholtz and Anders Karlhede. Half-filled lowest landau level on a thin torus. *Physical review letters*, 94(2):026802, 2005.
- [95] B Andrei Bernevig and Nicolas Regnault. Thin-torus limit of fractional topological insulators. *arXiv preprint arXiv:1204.5682*, 2012.
- [96] Lucila Peralta Gavensky, Gonzalo Usaj, and Nathan Goldman. Středa Formula for Floquet Systems: Topological Invariants and Quantized Anomalies from Cesàro Summation. *Phys. Rev. X*, 15:031067, Sep 2025.
- [97] Benjamin M. Fregoso. Average density of Bloch electrons in a homogeneous magnetic field: A second-order response. *Phys. Rev. B*, 113:085102, Feb 2026.
- [98] This equality holds only in the absence of poles and zeros of the Green's function at the chemical potential; see [27] for details.
- [99] The explicit lattice translational symmetry is broken in the presence of the homogeneous magnetic field. All the gauge invariant quantities, however have to preserve the translational symmetry. The elements of the Green's functions and the self-energy which are diagonal in space indices are gauge invariant and therefore are translational invariant [?].
- [100] In fact, for a Laughlin-type FCI state one may expect correlations to decay faster than exponentially.